JRA1

Site effects at sites with pronounced topography: overview & recommendations

Final Version (4.9.2014)

Jan Burjánek, Donat Fäh,
Swiss Seismological Service, ETH Zürich

Marta Pischiutta, Antonio Rovelli, Giovanna Calderoni,
INVG Rome

Pierre-Yves Bard,
ISTerre, Grenoble

NERA-JRA1 working group.

List of appendices:

- **Appendix A:** Empirical evidence of local seismic effects at KiK-net and Swiss sites with pronounced topography
- **Appendix B:** Digital elevation models, amplifications and polarization analysis of KiK-net and Swiss sites
- **Appendix C:** Digital elevation models and polarization analysis of Italian sites
- **Appendix D:** An overview of instrumented European sites with complex topography
- **Appendix E:** Polarization analysis for a typical 1D site
- **Appendix F:** Horizontal amplification on topography at selected broad-band stations of INGV seismic network

Citation: Burjanek, J., Fäh, D., Pischiutta, M., Rovelli, A., Calderoni, G., Bard, P.-Y., NERA-JRA1 working group (2014). Site effects at sites with pronounced topography: overview & recommendations, Research report for EU project NERA, 64 pp, doi: 10.3929/ethz-a-010222426.

Site effects at sites with pronounced topography: overview & recommendations

We present results of a joint effort undertaken in European project NERA -JRA1, which aims at establishing scientifically solid and practically acceptable propositions how to incorporate site effects in seismic hazard assessment at sites with pronounced topography. We first summarize what influences the site response at such sites most. We avoid the terminology "topographic site effect" as it is usually understood as a pure effect of surface geometry on ground motion, represented by models of homogeneous half space with a non-planar free surface. However, it has turned out that the observed amplifications at sites with pronounced topography could not be usually explained by the terrain geometry only, and are instead tightly linked with the local sub-surface structure, specifically the shear-wave velocity (e.g., Paolucci et al., 1999; Assimaki et al., 2005; Graizer, 2009; Glinsky and Betrand, 2011; Gallipoli et al., 2013). Thus results of models based on homogeneous substratum have limited application in real cases.

In this document, we overview recent results and sketch recommendations for practical applications. The key results have been published in the paper by Burjanek et al. (2014), henceforth BU14, which can be found in the Appendix A of this document. 25 instrumented sites with complex topography were identified in Switzerland and Japan based on quantitative DEM analysis (BU14). A detailed site characterization, including measured S-wave velocity profiles down to 30-200 m, is available for these sites, as well as empirical amplification functions relative to a derived reference rock profile (Edwards et al., 2013). We have focused on the sites classified as ridges, since the amplification effects due to topography are expected to be strongest at these locations (e.g., Maufroy et al., 2012; Lee et al., 2009). We checked the both polarization and directionality of ground-motion since a number of observational studies have found directional site effects at locations with pronounced topography (e.g., Bonamassa and Vidale 1991; Spudich et al. 1996; Del Gaudio and Wasowski, 2007; Burjanek et al. 2010; Massa et al., 2010; Pischiutta et al., 2010 and 2011; Panzera et al., 2011, Burjanek et al., 2012). By polarization we mean shortly linearity of the particle motion and by directionality concentration of the particle motion azimuths.

Since the total number of sites analyzed in BU14 is still relatively limiting, we tried to incorporate available results for Italian and Japanese K-NET sites as well (Appendices C, F). However, these studies present several limitations. We briefly summarize the main results here.

At first, both noise and earthquake recordings of 20 stations of Italian broadband network, located at sites with pronounced topography, were processed with polarization analysis (see Appendix C). The results of the polarization analysis could be directly compared with BU14 study, since the same method was applied. Some of the sites (9 in total, e.g., BULG, CERT, CLTB, CTI, GIB, ILLI, MAGA, MRB1, SSY) show strong polarization (linearity of the particle motion and directionality) at certain frequencies. The rest of the sites show weak, or no polarization (MAIM, MCEL). A band limited disagreement between the results for the noise and earthquake recordings is observed at number of sites (e.g., CERT, GIB, INTR, LADO, MAIM, SGTA, VULT). This might be addressed to strong directional sources in the ambient noise wavefield (see BU14 for the discussion). Nevertheless, we do not have neither measured shear wave velocity profiles nor observed amplification functions for these sites. However, we could state, that the

observed polarization is not solely linked to the terrain geometry (e.g., compare site MCEL and CLTB), thus subsurface structure has to play a role.

At second, an independent study of ground motion polarization and amplification was performed at a number of Italian sites (Appendix F). Some of the sites (ALJA, CERT, CLTB, ILLI, INTR, LADO, MAGA, SGTA) were included in the preceding study (see paragraph above). So that it is possible to compare the different polarization analysis, and especially find the potential link between the observed ground motion directionality and amplification. The results of the two different polarization estimates are in good agreement (compare Fig. 2 in Appendix E, with polar plots in Appendix C). The potential amplification was deduced from the comparison of the observed response spectra for a number of earthquakes and ground motion prediction model. In general, the directional amplification is observed at sites with strong ground motion polarization (CERT, CLTB, ILLI, MAGA). The recordings of the station INTR are probably affected by strong directional noise source (see Appendix C). The comparison was performed for very limited number of events (less than four), so it is impossible to make any conclusions. Moreover, we do not have measured shear wave velocity profiles for these sites. Nevertheless, even this limited study supports the link between amplification and ground motion directionality.

At third, Japanese K-NET sites were investigated in similar way as the KiK-net sites in BU14. Seven ridge sites were identified in the network by DEM analysis. However, we later found that some of the K-NET station coordinates published at Kyoshin website[1] are not correct (at least two of the seven sites are located some hundred meters from the reported position – not on the ridge anymore), so that we decided not to include these results in this document. We would like to emphasize here that this is not the case of the KiK-net stations.

The following statements related to the site soil classes and observed amplifications are based on the work done on 25 Swiss and Japanese sites, since the additional studies described in preceding paragraphs have limitations. EC8 Soil classification is based on measured Vs30. In the following, we summarize our main observations:

(1) We have not identified any general link between the geometrical features of the surface topography and the observed site response.

Observed amplifications can differ up to a factor of **20** for similar sites with comparable surface topography: this is a too large difference with respect to expected ground motion variability due to surface geometry only (Maximum factor of **2**, e.g. Assimaki et al., 2005; Lee et al., 2009). As an example compare sites SZOH34 and HASLI in Appendix B. To avoid any misunderstanding, we definitely do not claim that the geometry of the surface has no effect on the ground motion at all. The observation is just that the large systematic amplifications at topographic sites cannot be explained by surface geometry only.

(2) Subsurface velocity structure is variable even under sites with complex topography.

[1] http://www.kyoshin.bosai.go.jp/kyoshin/db/index_en.html?all

In our study EC8 soil classes ranging from A to D have been found. This might be seen as a trivial observation. However, some of the sites can be identified as outcropping rock sites by only looking at the borehole lithology log (e.g., see sites WKYH08, KGSH12, NARH01, YMGH15 in Table 2, BU14), but the Vs30 values correspond to velocity ranges of sediment sites. This shows the importance of shear-wave velocity measurements even at the rock outcrops. It has to be noted that the vast majority of numerical studies on topographic site effects have assumed shear-wave velocities larger than 1000 m/s.

(3) The amplification is controlled in first place by the sub-surface velocity structure.

The rock sites (EC8 class A) with pronounced topography studied here do not, on average, exhibit any systematic amplification. In particular, we do observe only weak amplification (factor <2) with respect to the reference rock condition at some sites, and in many cases a de-amplification. The amplification or de-amplification is almost frequency independent. On the other hand, the rest of the sites (non EC8 class A) present systematic frequency dependent amplifications (up to a factor of 20 in particular frequency bands) with respect to reference rock condition.

(4) The observed amplifications are correlated with ground motion polarization and directionality.

The amplified ground motion at non EC8 class A is found to be polarized and directional, i.e., ground motion vibrates in specific directions (see Figure 8 in BU14 and Appendix B). In particular, the frequency of the fundamental peaks in the amplification curves correlates with the frequencies where the ground motion becomes polarized and directional (see Figure 9 in BU14). This directionality is observed consistently in the both ambient vibration and earthquake recordings (see Figure 5 in BU14). The directionality and polarization of ground motion originate likely from the structure near the surface (<100 m, in most of the cases). This was demonstrated by polarization analysis of corresponding borehole recordings of the Japanese sites, which present neither directionality nor polarization (see Figure 10 in BU14).

Based on these observations, we conclude that strong systematic amplification observed at sites with pronounced topography is controlled by subsurface velocity structure, rather than the shape of the topography. The pure effects of surface geometry might be observed only at hard rock sites where the amplification due to the subsurface structure does not dominate the wave-field. Although, based on our observation, such effects do not seem to result in strong systematic amplification nor de-amplification (compared to effects due to subsurface velocity structure), they might appear for specific source locations (Lee et al., 2009). The conclusions are based just on analysis of 25 sites, so further studies are strongly required. Moreover, the unique physical model for the observed directional resonances has not been identified yet. The directionality might be in principle explained by 2D resonances. In particular, a presence of seismic impedance contrast (due to soft subsurface material) under 2D geometrical structure (e.g., ridge) could result in P-SV and SH normal modes like in 2D Alpine valleys (e.g., Ermert et al., 2014). However, it is sometimes difficult to relate observed directionality to surface geometry (e.g.,

sites SZOH34 and CERT in Appendix B and C, respectively). On the other hand, directional response might be caused by the fractured nature of the medium as well (Burjanek et al., 2012). Specifically, it seems that the bulk stiffness of the fractured rock mass could drop significantly in the direction perpendicular to the fractures. Thus the isotropic low velocity subsurface structure might not likely explain observed directionality. Nevertheless, it is necessary in the future to confirm these hypotheses by detailed field observations (e.g., fracture observations and characterization) and through numerical modeling.

Based on our findings, we can propose the following recommendations for local seismic effect evaluation at sites with pronounced topography:

(1) Seismic response can be hardly anticipated just from the terrain geometry.

Standalone analysis of a digital elevation model will not reduce uncertainty in hazard estimation at sites with pronounced topography. It could lead to severe underestimation of potential amplifications.

(2) Significance of amplification at a given site can be predicted at low-cost through non-invasive polarization analysis of the ambient noise wave-field.

Strong polarization of the horizontal component and high directionality of ambient vibrations (AV) are signatures of potentially strong site effect. In particular, the fundamental frequency and direction (direction where the strongest amplification occurs) can be estimated from AV. Although time-frequency polarization analysis (TFPA, Burjanek et al., 2010, 2012) was exclusively applied in BU14 to process ground motion data, even simpler directional H/V ratio could be applied as well. Nevertheless, TFPA outperforms directional H/V providing better directional resolution (see Figure 3.1 in Appendix D), and is also capable to detect non-directional site effect too (see Appendix E). We also stress here the problem of the strong local anthropogenic noise sources (i.e., industrial peaks), which represent a general problem in ambient vibration surveys. Ground motion generated from such sources are usually mostly harmonic, polarized and strongly directional (see, e.g., Figure 5 in BU14). Thus, presence of such sources can be easily confused with the directional site response. Since such sources usually have very narrow band spectra, it is possible to recognize them through analysis of the power spectral densities (estimated with methods preventing spectral leakage, e.g., without artificial smoothing, which smears the peaks).

(3) Efforts should be concentrated on retrieving subsurface velocity structure.

If a potential site-effect was identified from single station polarization analysis, it might be justified to measure the velocity structure. This should be obtained by direct measurements and not from the lithology of observed outcropping rock unit. This might present a challenge, since current geophysical methods are adapted more to situations with layered sediments (e.g., alluvial sediments). One has to be aware that exposed topographic sites are likely formed by

particular geomorphological processes (e.g., weathering), and could be, for example, strongly fractured. In case of fracturing, standard geophysical velocity measurements might fail.

(4) Detailed numerical modeling can reveal the joint effect of surface geometry and subsurface velocity structure.

A successful prediction of the local response of sites with pronounced topography needs a reliable shear wave velocity model representative of the site (i.e., a measured one). Detailed numerical modeling can subsequently reveal the joint effect of surface geometry and subsurface structure. However, for example, the presence of fractures could strongly affect the seismic response, which should be well represented in the numerical simulations.

The evaluation of the site response at site with pronounced topography can therefore be performed with the following procedure:

(i) Acquisition of ambient vibrations at multiple points at site of the interest to map the area for possible site-effects.

(ii) If the polarization analysis does not reveal near strong directionality or polarization of ground motion on the horizontal component of motion, the site is likely not prone to strong site effect (potential amplification is likely less than 2).

(iii) If the polarization analysis reveals a systematic polarization, an amplification could be expected. Further investigations are then recommended. This can include a temporary seismic station deployment to estimate directly the empirical amplification at the site. The measurements of the subsurface velocity structure present another option. Low shear-wave velocities clearly indicate potential site effect, which can be quantified through numerical modeling. Nevertheless, it is recommended to validate such numerical results with other seismic observations (e.g., with local site to reference spectral ratios – even performed with ambient vibrations).

Concluding recommendations to EC8 update

The NERA-JRA1 working group on topography expresses serious doubts about the relevancy of the topographic aggravation factor presently included in the EC8 recommendations. This tau "τ" coefficient is presently a) related to the sole surface geometry, b) frequency independent, and c) limited to maximum increase of 40%. In our study we have shown that the shear-wave velocity structure is much more important than the geometry of a site.

The review of available results (recorded data and numerical simulation) suggests that effects of pure topography are limited to a factor at most 2 for common topographic features; such a factor falls within

the variability range of all GMPEs used for the hazard assessment studies and derived design spectra. As the surface topography conditions are not taken into account in the derivation of GMPEs, it is very likely that such purely geometrical effects contribute to the variability "σ" of GMPEs: applying an additional "tau" coefficient opens the possibility of "double counting" the effect of surface topography. Moreover soil classification for soil A (here strictly defined by Vs values) is often based on lithology and can be strongly biased, mixing B, C, or even D class sites into class A. Therefore, the design spectrum for the rock class A already contains likely effects of softer material and is therefore conservative.

All available results also emphasize the frequency dependence of effects related to sites with pronounced surface topography, whatever its origin (pure geometry, i.e., local curvature, shallow shear-wave velocity structure or fracturing). This is not accounted for in the present EC8 formulation and might lead to an over- or under-estimation in particular frequency ranges. Finally, the limited EC8 values (+40% only) are not appropriate for the cases where significant site effects are observed on pronounced topography, which are not due to geometrical effects: in such cases, the amplification levels may reach factors up to 4 to 20 in particular frequency ranges, and the present EC8 recommendations may provide a dangerous illusion of security.

As a consequence, the majority of the members of the NERA-JRA1 working group on topography recommend to drop the "τ" coefficient as it is presently specified in EC8, and to follow the proposed site-specific procedure for cases where site-effects on pronounced topography may be suspected.

The same working group recommends the gathering of additional data through specific studies including systematic site surveys, in order to establish more robust conclusions.

References

Assimaki, D., Gazetas,G., & Kausel, E., 2005. Effects of local soil conditions on the topographic aggravation of seismic motion: parametric investigation and recorded field evidence from the 1999 Athens earthquake, Bull. seism. Soc. Am., 95, 1059–1089.

Bonamassa, O. & Vidale, J. E., 1991. Directional site resonances observed from aftershocks of the 18th October 1989 Loma Prieta earthquake, Bull. seism. Soc. Am., 81, 1945–1957.

Burjánek, J., Gassner-Stamm, G., Poggi, V., Moore, J. R., & Fäh, D., 2010. Ambient vibration analysis of an unstable mountain slope, Geophys. J. Int., 180, 820-828.

Burjánek, J., Moore, J.R., Yugsi-Molina, F.X., & Fäh, D., 2012. Instrumental evidence of normal mode rock slope vibration, Geophys. J. Int., 188, 559-569.

Burjánek, J., Edwards, B., & Fäh, D., 2014. Empirical evidence of local seismic effects at sites with pronounced topography: a systematic approach, Geophys. J. Int., doi: 10.1093/gji/ggu014, in press.

Del Gaudio, V., & Wasowski, J., 2007. Directivity of slope dynamic response to seismic shaking, Geophys. Res. Lett., 34, L12301.

Edwards, B., Michel, C., Poggi, V., & Fäh, D., 2013. Determination of site amplification from regional seismicity: application to the Swiss National Seismic Networks, Seismological Research Letters, in press, doi: 10.1785/0220120176.

Ermert, L., Poggi, V., Burjánek, J.,& Fäh, D. 2014. Fundamental and higher 2-D resonance modes of an Alpine valley, Geophys. J. Int., 198 (2), 795-811, doi:10.1093/gji/ggu072.

Gallipoli, M. R., Bianca, M., Mucciarelli, M., Parolai, S., & Picozzi, M., 2013. Topographic versus stratigraphic amplification: mismatch between code provisions and observations during the L'Aquila (Italy 2009) sequence, Bulletin of Earthquake Engineering, in press, doi:10.1007/s10518-013-9446-3.

Glinsky, N., & Bertrand, E., 2011. Numerical study of topographical site effects by a discontinuous finite element method. 4th IASPEI / IAEE International Symposium: Effects of Surface Geology on Seismic Motion, In CD. University of California Santa Barbara, CA, USA.

Graizer, V., 2009. Low-velocity zone and topography as a source of site amplification effect on Tarzana hill, California, Soil Dyn. Earthq. Eng., 29, 324–332.

Lee, S. J., Chan, Y. C., Komatitsch, D., Huang, B. S. & Tromp, J., 2009. Effects of realistic surface topography on seismic ground motion in the Yangminshan region of Taiwan based on the spectral-element method and LiDAR DTM. Bull. seism. Soc. Am., 99, 681–693.

Massa, M., Lovati, S., D'Alema, E., Ferretti, G., & Bakavoli, M., 2010. An experimental approach for estimating seismic amplification effects at the top of a ridge, and the implication for ground-motion predictions: the case of Narni (central Italy), Bull. seism. Soc. Am., 100, 3020-3034.

Panzera, F., Lombardo, G., & Rigano, R., 2011. Evidence of topographic effects through the analysis of ambient noise measurements, Seism. Res. Lett., 82, 413-419.

Paolucci, R., Faccioli, E., & Maggio, F., 1999. 3D response analysis of an instrumented hill at Matsuzaki, Japan, by a spectral method, J. Seism., 3, 191–209.

Pischiutta, M., Cultrera, G., Caserta, A., Luzi, L., & Rovelli, A., 2010. Topographic effects on the hill of Nocera Umbra, central Italy, Geophys. J. Int., 182, 977–987.

Spudich, P., Hellweg, M., & Lee, W.H.K., 1996. Directional topographic site response at Tarzana observed in aftershocks of the 1994 Northridge, California, earthquake: implications for mainshock motions, Bull. seism. Soc. Am., 86, S193–S208.

Appendix A

Empirical evidence of local seismic effects at KiK-net and Swiss sites with pronounced topography

Empirical evidence of local seismic effects at sites with pronounced topography: a systematic approach

Jan Burjanek[1], Benjamin Edwards[1], and Donat Fäh[1]

[1]Swiss Seismological Service, ETH, Zürich, Switzerland

Accepted 01/2014. Received 11/2013; in original form 06/2013.

Abbreviated title: Local seismic effects at topographic sites

Corresponding Author: Jan Burjanek
Swiss Seismological Service
Eidgenössische Technische Hochschule (ETH) Zürich
Sonneggstrasse 5
8092 Zurich, Switzerland
Email: burjanek@sed.ethz.ch

doi: 10.1093/gji/ggu014

Summary

The recent growth of seismic monitoring networks allows for systematic studies of local seismic effects at sites with pronounced topography. We applied a terrain classification method to identify such sites within Swiss and Japanese networks and compiled a dataset of high quality earthquake recordings. As a number of recent studies have found local effects to be directional at sites with strong topographic features, polarization analysis of particle motion was performed and azimuthally dependent resonant frequencies were estimated. The same procedure was also applied for available ambient vibration recordings. Moreover, average residuals with respect to ground motion prediction models for a reference bedrock were calculated to estimate the average amplification or de-amplification for each station. On one hand, observed amplifications are found to be tightly linked with ground motion directionality as estimated by polarization analysis for both earthquake and ambient vibration recordings. On the other, we found no clear relation between local topographic features and observed amplification, so the local sub-surface properties (i.e., shear wave velocity structure) seem to play the key role and not the geometry itself.

Keywords: Earthquake ground motions; Site effects; Wave propagation; Time-series analysis; Fourier analysis; Wavelet transform.

1. Introduction

The effects of surface topography geometry on seismic ground-motions have been discussed for a long time, and have been the topic of many instrumental and numerical investigations over the last four decades. However, their complexity, combined with the limitations of both geophysical investigation techniques and numerical simulation, made it impossible until now to properly include such effects in earthquake hazard assessment and risk mitigation policies. The understanding and quantification of site effects is an important aspect of seismic hazard analysis, particularly in the case of detailed site-specific analyses for critical structures. An important question is therefore whether, despite the modelling and investigation complexity, it is important to consider the topographic component of site amplification when performing seismic hazard analysis. Moreover, site effects related to surface geometry are usually linked to co-seismic landslides, which contribute significantly to earthquake damage (Marano et al., 2010).

A number of purely numerical studies have been produced, focusing mainly on the challenging task of introducing complex topography into wave propagation codes (e.g., Boore, 1972; Bouchon et al., 1996; Moczo et al., 1997; Komatisch et al. 1998). Such simulations generally suggest an amplification of ground-motion on mountain crests due to constructive interference of seismic waves within convex shapes, while at footslopes de-amplification of ground motion is expected due to scattering at concave shapes. Amplification/de-amplification factors of up to 2 are expected for very special cases (e.g., Assimaki et al., 2005; Lee et al., 2009), with the specific value depending on the geometry and on the reference site selection (e.g., Paolucci, 2002; Maufroy et al., 2012). However, cases of pronounced amplification evident in strong ground motion recordings have been reported at sites with specific topographic features (e.g., Davis and West, 1973; Tucker et al., 1984; Shakal et al., 1988; Spudich et al., 1996) while increased damage has been identified at such sites after earthquakes (e.g., Gazetas et al., 2002; Hough et al., 2010; McCrink et al., 2010). Although attempts have been made to explain such observations with the effect of the terrain geometry, these strong levels of observed amplification remain unexplained in most cases (e.g., Bouchon and Barker, 1996; Lovati et al., 2011). It has turned out that the observed amplifications cannot be explained only by the geometry of the topography, and are instead tightly linked with the local sub-surface structure, specifically the shear-wave velocity (e.g., Spudich and Barker, 1996; Paolucci et al., 1999; Assimaki et al., 2005; Glinsky and Betrand, 2011; Gallipoli et al., 2013). Nevertheless, the published observations present isolated case studies with different levels of investigations, thus it is difficult to find common conclusions.

Co-seismic landslides are of great significance in seismic risk studies, and are sometimes related to the influence of the soil and rock conditions and the surface geometry on incident ground motion (Sepúlveda et al., 2005). The seismic response of unstable rock slopes is not part of this paper, as we consider it as a very site-specific problem. The observed site effects on unstable rock slopes seem to be particular cases, e.g., amplification factors may reach values of up to 30 over very short distances (Burjánek et al, 2010; 2012) and purely geometrical effects seem to be almost negligible (Moore et al., 2011).

In this paper we follow a different strategy to previous studies. We do not focus on a single site, but rather perform a systematic study on a set of sites with pronounced topography. This is possible since the density of seismic networks has increased over recent years, with a number of stations located on pronounced topographic features. Moreover, homogeneous site characterization has been performed for various networks including geophysical investigation (e.g., KiK-net and K-NET in Japan, Swiss National Seismic Network, CHNet). We therefore present a systematic study of Swiss CHNet and Japanese KiK-net sites. A quantitative terrain classification of the sites was performed to select sites of interest in an objective way. The ground-motion recordings collected at these selected sites were subsequently analysed. Average amplification functions with respect to ground motion prediction models for a reference rock were calculated to estimate frequency-dependent amplification and de-amplification. Moreover we analyse the directionality of ground-motion since a number of observational studies have found directional site effects at locations with pronounced topography (e.g., Bonamassa and Vidale 1991; Spudich et al. 1996; Del Gaudio and Wasowski, 2007; Burjanek et al. 2010; Massa et al., 2010; Pischiutta et al., 2010 and 2011; Panzera et al., 2011, Burjanek et al., 2012). Thus we propose the polarization analysis of particle motion as an additional element of the ground motion characterization.

2. Data

2.1 Seismic Data

A number of instrumented sites with complex topography were identified in Switzerland and Japan. These regions present ideal situations to systematically study effects at such sites. Firstly, both Switzerland and Japan have rough topography and a relatively high density of seismic stations. Secondly, many of the Swiss permanent stations have a detailed site characterization including measured S-wave velocity profiles down to 30-100 m, and mean amplification functions relative to the Swiss reference profile are available for all stations (Fäh et al., 2009; Edwards et al., 2013). Shear-wave velocity profiles are also available for all KiK-net stations down to at least 100 m. Finally, ground motion prediction models are available for both Japan and Switzerland with respect to precisely derived reference velocity profiles (Poggi et al., 2011; 2013). Both weak-motion earthquake and ambient vibrations recordings were collected for the Swiss network. Only earthquake recordings were available for the KiK-net stations.

2.2 Digital Elevation Model

The 'Advanced Spaceborne Thermal Emission and Reflection Radiometer' (ASTER) 'Global Digital Elevation Model Version 2' (GDEM V2) was used to represent the terrain's surface. The model is available at no charge as a set of geo-referenced images. The Digital Elevation Model (DEM) accuracy, in terms of the standard deviation with respect to the reference model, is reported to be in the range of 7-14 m depending mainly on land cover (i.e., the DEM is less accurate in the areas covered by woods). The images are referenced by latitude/longitude (WGS84) with a posting interval of 1 arc-second, which is roughly 30 m for the areas of interest.

3. Methods

3.1 Digital Elevation Model Analysis

In order to characterize the surface geometry of a given site, we adopted a classification scheme proposed by Weiss (2001). The scheme is based on the so called Topography Position Index (TPI), which is defined as a difference between the actual value of the elevation *H* at given location [*x*, *y*] and mean elevation of the neighbouring area *A*:

$$TPI(x,y) = H(x,y) - \int_A H(x,y)dS \Big/ \int_A dS \,. \qquad (1)$$

The area *A* should be centred at the point [*x*, *y*]. Both the size and the shape of the neighbouring area have to be defined in advance, depending on the specific application. In general, there is no constraint on both values. We use a square area for simplicity. The size of the area, however, presents a more fundamental issue. Surface topography has a self-affine nature (e.g., Turcotte, 1997), so it is very difficult to define a general characteristic length scale. For this reason, the choice of scale depends on the specific use. For example, in our case, we are interested in ground-motions in a characteristic frequency-band (or wavelength) at a given site. Such a frequency-band can be represented by a wavelength range, assuming a seismic velocity profile under the site. As these characteristic wavelengths are of principal interest, one should consider them in the selection of length scales for the topography classification. Unfortunately, since the seismic velocity structure is very variable in the uppermost part of crust and generally not known, it is impossible to define general wavelengths of interest for such seismological application. Moreover, the relation between seismic wavelengths and classification scales is not trivial and, for example, depend on the steepness of the slope.

Our final terrain classification follows Weiss (2001) and is based on the combination *TPI* and *Slope* values at given location. The *Slope* value is defined as a local steepest slope-angle γ, i.e., a magnitude of gradient:

$$\gamma(x,y) = \tan^{-1}\sqrt{\left[\frac{\partial H(x,y)}{\partial x}\right]^2 + \left[\frac{\partial H(x,y)}{\partial y}\right]^2} \,. \qquad (2)$$

In particular, *TPI* at a particular location is compared to the standard deviation σ_{TPI} of the *TPI* over the entire region. The slope value is used to distinguish between flat areas and areas in the middle of a slope, both of which have TPI close to zero. The definition of the different classes is presented in Table 1.

Here we briefly describe the technical details of the procedure, which are related to a specific DEM (ASTER GDEM in this case). At first, a region of 500x500 arc-seconds surrounding the seismic station was cut out from the DEM, as the analysis of the complete DEM would result in heavy calculations. Secondly, the DEM was smoothed using a 3x3 pixel (approximately 90x90 m) moving average to avoid small-length scale artefacts in the DEM. Thirdly, since the ASTER GDEM is saved in the geographic coordinate system

(WGS84) it is necessary to make a transformation to a Cartesian coordinate system to simplify the calculations of terrain parameters (*Slope*, *TPI*). Thus the DEM was converted to Universal Transverse Mercator coordinate system. Finally, the area of 8x8 km surrounding the seismic station was cut out from the converted image. This procedure was performed for all 689 KiK-net locations. As the KiK-net network covers more or less uniformly the entirety of Japan, different terrain types are sampled: the Japanese terrain morphology is therefore well represented by the DEM sub-selection. By performing several tests, we found that the total area analysed is sufficient for a stable definition of the standard deviation σ_{TPI}, which is used for the terrain classification (see Table 1). An example of the terrain classification using ASTER GDEM is presented in Figure 1 using a length scale of 1020 m for defining the area A. The influence of the selected length scale is presented later. The same procedure was applied for the station locations of CHNet. The value of standard deviation σ_{TPI} estimated for Japan was also applied for the Swiss sites to keep results consistent. Moreover, in case of Japan, almost 700 locations were analysed compared to 20 sites in Switzerland, thus σ_{TPI} estimated for Japan is more robust (i.e., a diversity of terrains was better sampled in Japan than in Switzerland).

3.2 Ground motion analysis

Several methods were applied to recorded ground motion. At first, particle motion analysis was applied to both recorded ambient vibration and earthquake recordings. Secondly, an earthquake spectral fitting procedure was utilized to isolate site effects.

3.2.1 Particle motion analysis

Several methods exist for the analysis of the directional site effects. Spudich et al. (1996) introduced directional site-to-reference spectral ratios (SRSR) for the estimation of the relative amplification depending on both frequency and azimuth. This method has been widely applied (e.g., Pischiutta et al., 2010; Massa et al., 2010), however, it requires a reference station, which is not always available. Therefore, directional non-reference H/V spectral ratios (HVSR) have been also applied in past studies (e.g., Del Gaudio and Wasowski, 2007). Whereas HVSR has been commonly applied on both earthquake and noise recordings, SRSR has been primarily used with earthquake recordings. Nevertheless, the SRSR method can also be applied to noise recordings if it can be assured that the noise generating sources (for frequencies of interest) are far from the site with respect to the distance between the site and the reference station (Roten et al., 2006; Burjanek et al., 2012). In this work, we focus on the non-reference methods, as a reference station is not available for most of the sites.

Recently, Burjanek et al. (2010) introduced time-frequency polarization analysis (TFPA), which is based on the combination of complex polarization analysis (Vidale, 1986) and the continuous wavelet transform (CWT). It can be viewed as a generalization of the directional HVSR method. Three polarization parameters are retrieved: 1) the azimuth of the major polarization axis, or strike, measured in degrees from North; 2) tilt of the major axis, or dip, measured in degrees downward from the horizontal; and 3) ellipticity, defined as the ratio between the length of the semi-minor and semi-major axes such that zero implies linear particle motion, while 1 implies circular particle motion. All three polarization parameters vary with both time and frequency. Usually, we assume that observed ambient

vibrations are quasi-stationary (i.e., noise properties do not change systematically on the time scale of the experiment – typically a few hours), and analyse the relative occurrence of polarization parameters. In particular, histograms of polarization parameters are constructed over time for each frequency. Polar plots are then adopted for the presentation of results, which illustrate combined angular and frequency dependence. While directional HVSR can be used to estimate just the polarization azimuth (orientation in horizontal plane), the TFPA method also provides information on the inclination of the particle motion (dip). Moreover, the use of CWT maintains optimum time-frequency resolution, which can be smoothly regulated through adjustment of the mother wavelet.

We found that the observed histograms of strike and dip can be fit by the Wrapped Cauchy distribution for given frequency. The Wrapped Cauchy distribution is a circular distribution, i.e., is used to describe periodic quantities (like angles). It is a symmetric distribution and is characterized by mean and concentration value. An example of Wrapped Cauchy distributions is provided in Figure 2. The concentration parameter ρ measures the scatter. While ρ=0 results in the uniform distribution (see Fig. 2), ρ=1 results in the Dirac delta function. Both mean and concentration can be estimated for a given frequency, for example, by applying a maximum likelihood method. This allows for a quantitative analysis of polarization analysis results. In other words, the frequency dependent level of directionality is mapped to the frequency dependent concentration value (ρ=0 signifies no directionality, while ρ≈1 means completely directional). Note that the concentration value is independent of the ellipticity value defined earlier – motion can be polarized most of the time (i.e., low ellipticity), but the orientation of this polarized motion can vary in time (i.e., low concentration).

3.2.2 Spectral analysis of earthquake recordings

Elastic amplification functions and near-surface attenuation terms (κ_0 , Anderson and Hough, 1984) were determined for the studied sites though the empirical spectral modelling approach of Edwards et al. (2013). Combined, these terms form the anelastic amplification function describing the influence of the upper soil or rock layers on the wave-field for each site. The employed method robustly isolates the site contribution through a multiple stage non-linear regression. The inversion is stabilized through a parametric description of the source and path: a Brune (1970) ω^2 point-source model is assumed for small to moderate (M<6) events at sufficient distance, while intrinsic and geometrical attenuation is accounted for using frequency dependent exponential decay and frequency independent $1/R^{\lambda}$ type spreading respectively. Moment magnitudes, independently determined by the USGS for Japan or the Swiss Seismological Service for Switzerland are used to decouple the trade-off between source and site. The use of non-parametric site terms allow for the consideration of 2- or 3D effects and the influence of surface waves. Through this approach, consistently observed site specific effects are extracted relative to a reference model (Poggi et al., 2011; 2013). Exhaustive description of the method and extensive testing, showing consistency with existing methods such as 1D-SH and site-to-reference spectral ratios, can be found in Edwards et al. (2013).

4. Results

4.1 DEM analysis

DEM analysis was performed to characterize the stations' locations. The key issue of the DEM analysis is the selection of the appropriate *scale*, represented by the size of the spatial window which defines *TPI*. As the characteristic wavelengths are generally not known for the investigated sites, a multi-scale analysis is required. In other words, several windows of different size (area A in Eq. 1) are applied, so the classification is not a single index, but a set of numbers, depending on the scale (size of the window). As a result, such classifications cannot be directly linked to seismic amplification unless the relation to seismic wavelengths is known. This is generally a difficult task due to the limited knowledge of the sub-surface velocity structure and potential 3D wave propagation effects. The influence of the selected *scale* is presented in the Figure 3. As expected, except for flat areas, on the very top of sharp crests and at the very bottom of sharp V-shaped valleys (i.e. for strictly self-similar structures), site classification strongly depends on the scale. Thus the classification of all Japanese and Swiss sites was performed with five different scales (120m, 220m, 500m, 1020m, and 2020m). By scale we always mean the size of square spatial window (area *A* in Eq. 1). The distribution of the KiK-net sites according to terrain classes at 1020m and 500m is plotted in Figure 4. A weak correlation was found between the different scales, which decreases with increasing scale ratio. For example, most of the ridge sites identified at scale 2020 m are also identified as ridges using the 1020 m scale. We focus here on the sites classified as ridges, since the amplification effects due to topography are expected to be strongest at these locations (e.g., Maufroy et al., 2012; Lee et al., 2009). Moreover, the classification of the ridge is less scale dependent, especially in the vicinity of mountain crests (see Figure 3). Nevertheless, the number of such sites naturally still increases with decreasing scale. We limited our study to sites identified as ridges only at scales of either 1020m or 2020m for which we can expect effects over a wide frequency band. Assuming a hill's height of a hundred meters and shear wave velocities in range of 1500-3000 m/s, which are usually considered in numerical studies of topographic site effects, the lower limit of this range is 0.5-2Hz. In particular, we decided to study only sites with the most pronounced topographic features in mountainous regions to reduce the analysis to fewer sites, but with deeper insight. The selected 25 KiK-net and Swiss sites are listed in Table 2 together with available site information.

4.2 Ground motion analysis at selected sites

In case of the Swiss stations, polarization analysis was performed on both earthquake and ambient vibration recordings. Windows of two hours of ambient vibration recordings were cut out from continuous recordings for each station. These time windows usually start after midnight to prevent (as much as possible) the recording of human activity. Recordings were checked visually for any transients and only stationary signals were processed. In addition, a number of earthquake recordings were selected for each site (20 events on average). These are recordings of local events (epicentral distance less than 50 km, local magnitudes M_L in range of 2 to 4) with good signal to noise ratio. Seismograms were merged to a single three-component time series and processed in the same way as ambient vibrations. Complete seismograms entered the analysis; no windowing was applied, so that recordings include few seconds of ambient noise at the beginning. However, the duration of these ambient vibrations is small compared to duration of the earthquake ground motion.

A comparison of the concentration of the strike angle for four representative sites (FLACH, AIGLE, BALST, and HASLI) is shown in Figure 5. At station FLACH the ground motion is directional (a peak in concentration of the strike angle exists) at 4.5 Hz. In this case a good agreement between the noise and earthquake recordings was also apparent. A similar agreement was found for station AIGLE, where the ground-motion becomes directional at 3.5 Hz, however, other peaks in concentration also appear in the case of ambient vibrations (2.3, 25 Hz). These two peaks likely have an industrial origin. The stations FLACH and AIGLE represent sites with directional site response. No peaks in concentration are observed at station BALST for both earthquake and ambient vibration recordings, while at station HASLI one can see only a peak in concentration close to 16.5Hz. This peak has a likely industrial origin (probably related to AC frequency of 16.7 Hz of the Swiss rail network which is operating less than 500 m from the site). The stations BALST and HASLI represent sites with an isotropic site response. Due to the similar results obtained for earthquake recordings and ambient vibrations, a simple ambient vibration measurement can be applied to assess possible amplification effects at rock-slope sites (see below). Nevertheless, industrial peaks represent a general problem in ambient vibration surveys. Moreover, such ground motion generated from one mostly harmonic source is observed to be usually strongly directional, thus can easily bias our polarization analysis. A careful analysis of ambient vibration time series is therefore necessary to prevent confusing the directional site response with the directionality of strong industrial sources. Since such sources usually have very narrow band spectra, it is possible to recognize them through analysis of the power spectral densities. Furthermore, since the ambient vibrations in this study were recorded during the night, and have relatively long duration (2 hours), the results presented here represent a rather good end case.

Only earthquake recordings are available at KiK-net stations. For the polarization analysis the data selection includes both regional and local events (60 events per site on average; epicentral distance less than 100 km; magnitude M_{JMA} in range of 2 to 6.5). Both surface and borehole recordings were analysed.

The empirical spectral modelling approach was performed for earthquake recordings on both KiK-net and Swiss stations. The earthquake recordings are not necessarily the same as for the polarization analysis, since there are different selection criteria for the ground motion in case of the spectral fitting (e.g., sufficient number of stations per event, point source approximation, S wavefield only). We are not interested in the source properties in this study, so only the non-parametric site-term is of our interest. This site term represents the frequency dependent relative amplification with respect to a precisely derived reference profile (Poggi et al., 2011; 2013) and can be viewed as an analogue to the site-to-reference spectral ratio (Edwards et al., 2013). Amplification functions were not estimated for the sites EHMH08, KGSH12, and CHBH16, because of a limited amount of suitable recordings at these sites.

The results for all sites are provided in the electronic appendix (Appendix B of this document). We summarize here the main findings by presenting results for two representative sites. At first, results for the Swiss site BALST are presented in Figure 6. Station BALST is a hard-rock site (with travel-time average shear wave velocity in the upper 30 m (Vs30) of 1348 m/s) located just at the edge of a 300 m high limestone cliff (Fig. 6a). A topographic effect is expected here. However, we do not observe any systematic amplification at this site (Fig. 6c). Moreover we observe almost no directionality of the ground motion (Fig. 6b). The concentration of the strike angle remains low (Fig. 6c) at all frequencies,

and the ellipticity follows more or less the constant value of about 0.4 (Fig. 6d). Results for a KiK-net site YMGH15 are presented in Figure 7. Station YMGH15 is located on a 100 m high hill (Fig. 7a).The site has been classified as EC8 class B with Vs30=549 m/s, while the borehole lithology log shows layers of weathered schist. The amplification curve at this site has a peak at 6 Hz (Fig. 7c), and the amplification reaches factor of 4 with respect to the reference profile. Moreover, at the same frequency of 6 Hz the strike angle concentrates at 175° (Fig. 7b) and the ellipticity drops below 0.1 (Fig. 7d). The concentration of the strike at 6 Hz is relatively high, reaching 0.7 (Fig. 7c). Site YMGH15 therefore represents a site with a strong directional site effect.

The strike concentration and ellipticity mode curves for all sites are presented in Figure 8. Sites which have been assigned Eurocode 8 soil class A (EC8 A, see Table 2) are distinguished by different colour from the remaining sites. In case of EC8 A sites, the ellipticity mode curves are flat and remain in the range 0.3-0.4 (black curves, Fig 8a). The strike concentrations for the EC8 A sites remain below 0.3 (black points, Fig 8b), except at Swiss sites AIGLE and MUO. On the other hand, most of the other sites (non EC8 A) present different local minima in their ellipticity curves: dropping down to 0.1 (red curves, Fig 8a). Also concentrations of the strike reach higher values (up to 0.7) with respect to EC8 A sites (red points, Fig 8b). We define three levels of directional site effects: 1) strong directional site effect (clear peak in strike concentration>0.4); 2) weak directional site effect (clear peak in strike concentration ≈0.3-0.4); 3) no directional site effect (no clear peaks in strike concentration<0.3). We also take into account the existence of local minima in ellipticity. A strike concentration of 0.4 means that the preferential direction is observed approximately 5 times more frequently than the perpendicular one, i.e. clear directionality. Strike concentrations below 0.3 (still the preferential direction is 3 times more frequent) are difficult to interpret, as the ellipticity does not show any local minima for most of the cases, i.e. particle motion is far from linear. The results of such directionality classification are presented in Table 2 (colour code of the 6^{th} column). Although such a classification can be considered arbitrary (the border between weak and non-existing directional site effects is especially weak, e.g., OITH10, AICH07), it clearly highlights the link between strong amplification and ground motion directionality.

Finally, we noticed that the frequency of the fundamental peaks (f_0) in the amplification curves correlates with the frequencies where the ground motion becomes directional (e.g., Fig. 7c). Thus we manually picked and compared the frequencies of the peaks in amplification functions and strike concentration functions for non EC8 A sites showing strong peaked directionality (see Table 2). The result of this comparison is presented in Figure 9. The two measures of f_0 correlate very well. We do not provide any pick for the station NARH01, as the amplification function presents only a very broad peak (width of 10 Hz). We do not have any explanation for such behaviour, since it would require detailed site specific analysis. Moreover, we do not identify any correlating peaks at Swiss stations STEIN and SLE. We also do not provide any interpretation for the sites with weak directional effects (see Table 2), since we could not simply identify other common features. Nevertheless, some of the weak peaks in the strike concentration seem to be related to an amplification peak at these sites, but not always.

5. Discussion

We briefly summarize and discuss our observations. The rock sites (EC8 class A) with pronounced topography studied in this paper do not, on average, exhibit any systematic amplification. In particular, we do not observe any systematic residuals with respect to the reference ground motion prediction model nor any directionality of the motion. Nevertheless, the pure effects of surface geometry are usually reported to be source dependent (especially with respect to the source location – e.g., Maufroy et al., 2012; Lee et al., 2009), so they might be averaged out in our amplifications functions. On the other hand, the rest of the sites (non EC8 class A) present systematic frequency dependent amplifications with respect to the two reference ground motion models (the reference ground model for Japan and Switzerland is not the same). Moreover, these observed site effects are found to be directional, i.e., ground motion vibrates in specific directions. This directionality is observed in the both ambient vibration and earthquake recordings, thus seems to be source independent. Although the distribution of back-azimuths is not optimum at all sites in case of earthquakes recordings, the observed directionality cannot be linked to the source properties. To demonstrate this, we compare the results of the polarization analysis for the borehole and surface recordings at KiK-net sites in Figure 10. The borehole recordings show consistently frequency-independent ellipticity (black curves, Fig. 10a), and low concentration (<0.2) of the strike angle (black points, Fig. 10b). So the directionalities diminish in the borehole recordings. The results for the borehole recordings are strikingly similar to the surface recordings of the hard rock sites.

Two Swiss stations (AIGLE, MUO) stick out slightly from the described scheme. Station AIGLE represents a peculiar case. It has relatively high Vs30 of 1243 m/s, but presents directionality and de-amplification in the same frequency band with respect to the reference model. We do not have any explanation at the moment. However the station is located in a bunker about 20 m below the surface and it might be that the station is influenced by this construction. Station MUO also presents a specific site response. In particular the ground motion is polarized and directional at 1.5 Hz, and the high frequency ground motion is remarkably attenuated. The site can be potentially unstable, since it carries similar signs at previously studied unstable rock slopes (Burjanek et al., 2010; 2012). Moreover the S wave velocity measurements characterizing this site were not taken exactly at the location of the seismic station, but tens of meters away. Thus, taking into account rapid variation of the subsurface structures within unstable rock slopes, the true velocity at site could be different. On the other hand, some non EC8 A sites show just weak amplification (e.g., STEIN, SLE). For example, station STEIN is classified as EC8 B site where class B refers to the location of the station several meters below the ground surface in rock and Vs30=383 m/s that refers to the free surface. No strong amplification and no directionality of ground motion are observed. This might be explained by station's location below the ground surface.

Finally, we have not identified any link between the surface topography and the observed response at studied 25 sites. Observed amplifications differ by factor of 20 for some site couples with comparable topography: a large difference with respect to expected ground motion variability due to surface geometry only (factor of 2, e.g. Lee et al., 2009). Therefore, the amplification is controlled in first place by the sub-surface velocity structure. Although the effect of geometry is present, it cannot be simply

decoupled from the site response. The observed directionality cannot be easily related to the terrain characteristics (e.g., aspect angle). Moreover, all terrain characteristics are scale dependent, and thus strongly non-unique, omitting the subsurface velocity structure. Any future seismic site characterization of locations with complex geometry must have to account for the sub-surface velocity structure. It is interesting that some of sites can be identified as outcropping rock sites looking at the borehole lithology log (e.g., WKYH08, KGSH12, NARH01, YMGH15), however, the Vs30 values correspond to sediment sites. This shows the importance of the shear wave velocity measurements even at the rock outcrops. Nevertheless, all complexities mentioned in the previous paragraph suggest that observed site effects cannot be addressed just by simplified site classes (even based on Vs30 measurement). On the other hand, the response of the site can be evaluated quickly through passive seismic measurements, e.g., by ambient vibration surveys. In particular, sites presenting no polarization or directionality of ground motion are likely subjected, if at all, to weak site effects. On the other hand, strong site effects can be expected in the case of observations of polarized and directional ground motion.

6. Conclusions

Strong systematic amplification observed at sites with pronounced topography presented in this study is controlled by subsurface structure, rather than shape of the topography. The pure effects of surface geometry might be observed only at hard rock sites where the amplification due to the subsurface structure does not dominate the wavefield. Although, based on our observation, such effects do not seem to result in systematic amplification nor de-amplification, they might appear for specific source locations. The subsurface structure was found to be variable under the studied sites: even sites with rock outcrops presented a strong gradient of the shear wave velocity with depth. Thus the seismic hazard estimate at sites with pronounced topography requires a detailed knowledge of the subsurface; especially shear wave velocity structure and internal structure, not only in case of instable rock slopes (Burjanek et al., 2011). Studies based exclusively on the terrain topography have almost no chance to capture the site effects correctly. It is also impossible to define characteristic wavelengths from the terrain only, since the surface topography has a self-affine nature.

The observed amplifications are correlated with ground motion directionality. Although a unique physical mechanism has not been discovered yet, ground motion directionality can be viewed as an indication of strong site effects. Since such directionality is also observed in a consistent way in the ambient vibration wavefield, noise measurements could therefore be used in the future for a quick characterization of topographic sites.

In terms of seismic hazard, the present study suggests that efforts should be concentrated on modelling amplification due to subsurface structure rather than topographical effects. An important conclusion of this study is that the significance of amplification at a given site can be predicted at low-cost through non-invasive polarization analysis of the ambient noise wavefield. Whilst such approaches are common in microzonation studies using classical HVSR approaches, the improved TFPA approach of Burjanek et al. (2010) can provide further information as to the likelihood of amplification phenomena occurring at a given site, even before more complex array based approaches are undertaken. For instance, in the case

of flat HVSR, without directionality or ellipticity (all of which are obtained using a single sensor), we can assume that site effects will not be significant, whilst in the case that one or more of these indicators shows a peak, that strong amplification may affect the site.

Ultimately, we do not state that the geometry of the surface has no effect on the ground motion. A successful prediction of the local response of sites with pronounced topography has an origin in the availability of a reliable shear wave velocity model representative of the site (i.e., a measured one). Detailed numerical modelling can subsequently reveal the joint effect of surface geometry and subsurface structure. The conclusions of this study are based just on analysis of 25 sites, so the further studies are required together with more physical insight based on numerical modelling.

7. Acknowledgements

We are indebted to Vera Pessina for helpful discussions and suggestions on the DEM classification. We thank Marco Stupazzini, and an anonymous reviewer for constructive comments and helpful suggestions. We thank the National Research Institute for Earth Science and Disaster Prevention, Japan (NIED) for making waveform and velocity profile KiK-net data available. This research is part of the EU project NERA (Network of European Research Infrastructures for Earthquake Risk Assessment and Mitigation, task JRA1 – 'Waveform modelling and site coefficients for basin response and topography'). The study is also funded in part by the Swiss Federal Nuclear Safety Inspectorate. Wavelet software used in the polarization analysis was provided by C. Torrence and G. Compo, available at http://paos.colorado.edu/research/wavelets/.

8. References

Anderson, J.G., & Hough, S. E., 1984. A Model for the Shape of the Fourier Amplitude Spectrum of Acceleration at High-Frequencies, Bull. seism. Soc. Am., 74, 1969-1993.

Assimaki, D., Gazetas,G., & Kausel, E., 2005. Effects of local soil conditions on the topographic aggravation of seismic motion: parametric investigation and recorded field evidence from the 1999 Athens earthquake, Bull. seism. Soc. Am., 95, 1059–1089.

Bonamassa, O. & Vidale, J. E., 1991. Directional site resonances observed from aftershocks of the 18th October 1989 Loma Prieta earthquake, Bull. seism. Soc. Am., 81, 1945–1957.

Boore, D. M., 1972. A note on the effect of simple topography on seismic SH waves, Bull. Seism. Soc. Am. 62, 275-284.

Bouchon, M., & Barker, J. S., 1996. Seismic response of a hill: the example of Tarzana, California, Bull. seism. Soc. Am., 86, 66–72.

Bouchon, M., Schultz, C., & Toksoz, M., 1996. Effect of three-dimensional topography on seismic motion, J. Geophys. Res., 101, 5835–5846.

Brune, J. N., 1970. Tectonic stress and spectra of seismic shear waves from earthquakes, J. Geophys. Res., 75, 4997–5010.

Burjánek, J., Gassner-Stamm, G., Poggi, V., Moore, J. R., & Fäh, D., 2010. Ambient vibration analysis of an unstable mountain slope, Geophys. J. Int., 180, 820-828.

Burjánek, J., Moore, J.R., Gassner-Stamm, G., & Fäh, D., 2011. Seismic response of unstable mountain rock slopes: Topographic site effect?. 4th IASPEI / IAEE International Symposium: Effects of Surface Geology on Seismic Motion, In CD. University of California Santa Barbara, CA, USA.

Burjánek, J., Moore, J.R., Yugsi-Molina, F.X., & Fäh, D., 2012. Instrumental evidence of normal mode rock slope vibration, Geophys. J. Int., 188, 559-569.

Davis, L. L., & West, R., 1973. Observed effects of topography on ground motion, Bull. seism. Soc. Am., 63, 283–298.

Del Gaudio, V., & Wasowski, J., 2007. Directivity of slope dynamic response to seismic shaking, Geophys. Res. Lett., 34, L12301.

Edwards, B., Michel, C., Poggi, V., & Fäh, D., 2013. Determination of site amplification from regional seismicity: application to the Swiss National Seismic Networks, Seismological Research Letters, in press, doi: 10.1785/0220120176.

Fäh, D., Fritsche, S., Poggi, V., Gassner-Stamm, G., Kästli, P., Burjanek, J., Zweifel, P., Barman, S., Clinton, J., Keller, L., Renault, P., & Heuberger, S., 2009. Determination of Site Information for Seismic Stations in Switzerland, Swiss Seismological Service Technical Report: SED/PRP/R/004/20090831, for the Swissnuclear Pegasos Refinement Project.

Gallipoli, M. R., Bianca, M., Mucciarelli, M., Parolai, S., & Picozzi, M., 2013. Topographic versus stratigraphic amplification: mismatch between code provisions and observations during the L'Aquila (Italy 2009) sequence, Bulletin of Earthquake Engineering, in press, doi:10.1007/s10518-013-9446-3.

Hough, S. E., Altidor, J. R., Anglade, D., Given, D., Janvier, M. G., Maharrey, J. Z., Meremonte, M., Mildor, B. S.-L., Prepetit, C., & Yong, A., 2010. Localized damage caused by topographic amplification during the 2010 M7.0 Haiti earthquake, Nat. Geosci., 3, 778-782.

Glinsky, N., & Bertrand, E., 2011. Numerical study of topographical site effects by a discontinuous finite element method. 4th IASPEI / IAEE International Symposium: Effects of Surface Geology on Seismic Motion, In CD. University of California Santa Barbara, CA, USA.

Komatitsch, D., & Vilotte, J. P., 1998. The spectral-element method: an efficient tool to simulate the seismic response of 2D and 3D geological structures, Bull. seism. Soc. Am. 88, 368–392.

Lee, S. J., Chan, Y. C., Komatitsch, D., Huang, B. S. & Tromp, J., 2009. Effects of realistic surface topography on seismic ground motion in the Yangminshan region of Taiwan based on the spectral-element method and LiDAR DTM. Bull. seism. Soc. Am., 99, 681–693.

Lovati, S., Bakavoli, M. K. H., Massa, M., Ferretti, G., Pacor, F., Paolucci, R., Haghshenas, E., & Kamalian, M., 2011. Estimation of topographical effects at Narni ridge (Central Italy): comparisons between experimental results and numerical modeling. Bull. Earthquake. Eng., 9, 1987-2005, doi:10.1007/s10518-011-9315-x.

Maufroy, E., Cruz-Atienza, V. M., & Gaffet, S., 2012. A robust method for assessing 3-D topographic site effects : a case study at the LSBB Underground Laboratory, France, Earthquake Spectra, 28, 1097-1115, doi:10.1193/1.4000050.

Marano, K. D., Wald, D.J., & Allen, T.I., 2010. Global earthquake casualties due to secondary effects: a quantitative analysis for improving rapid loss analyses, Nat. Hazards, 52, 319-328, doi:10.1007/s11069-009-9372-5.

Massa, M., Lovati, S., D'Alema, E., Ferretti, G., & Bakavoli, M., 2010. An experimental approach for estimating seismic amplification effects at the top of a ridge, and the implication for ground-motion predictions: the case of Narni (central Italy), Bull. seism. Soc. Am., 100, 3020-3034.

Moczo, P., Bystricky, E., Kristek, J., Carcione, J. M., & Bouchon, M., 1997. Hybrid modelling of P-SV seismic motion at inhomogeneous viscoelastic topographic structures. Bull. seism. Soc. Am., 87, 1305-1323.

Moore, J.R., Gischig, V., Burjánek, J., Loew, S., & Fäh, D., 2011. Site effects in unstable rock slopes: dynamic behavior of the Randa instability (Switzerland), Bull. seism. Soc. Am., 101, 3110-3116.

Panzera, F., Lombardo, G., & Rigano, R., 2011. Evidence of topographic effects through the analysis of ambient noise measurements, Seism. Res. Lett., 82, 413-419.

Paolucci, R., 2002. Amplification of earthquake ground motion by steep topographic irregularities. Earthquake Eng. Struct. Dyn., 31, 1831–1853. doi: 10.1002/eqe.192.

Paolucci, R., Faccioli, E., & Maggio, F., 1999. 3D response analysis of an instrumented hill at Matsuzaki, Japan, by a spectral method, J. Seism., 3, 191–209.

Pischiutta, M., Cultrera, G., Caserta, A., Luzi, L., & Rovelli, A., 2010. Topographic effects on the hill of Nocera Umbra, central Italy, Geophys. J. Int., 182, 977–987.

Pischiutta, M., Rovelli, A., Vannoli, P., & Calderoni, G., 2011. Recurrence of horizontal amplification at rock sites: a test using H/V based ground motion prediction equations. 4th IASPEI / IAEE International Symposium: Effects of Surface Geology on Seismic Motion, In CD. University of California Santa Barbara, CA, USA.

Poggi, V., Edwards, B., & Fäh, D., 2011. Derivation of a reference shear-wave velocity model from empirical site amplification, Bull. seism. Soc. Am., 101, 258-274.

Poggi, V., Edwards, B., & Fäh, D., 2013. Reference S-wave velocity profile and attenuation models for ground-motion prediction equations: application to Japan, Bull. seism. Soc. Am., in press.

Roten, D., Cornou, C., Fäh, D., & Giardini, D., 2006. 2D resonances in Alpine valleys identified from ambient vibration wavefields, Geophys. J. Int., 165, 889–905.

Sepúlveda, S. A., Murphy, W., Jibson, R. W., & Petley, D. N., 2005. Seismically induced rock slope failures resulting from topographic amplification of strong ground motions: The case of Pacoima Canyon, California, Eng. Geol., 80, 336–348, doi 10.1016/j.enggeo.2005.07.004.

Shakal, A., Huang, M., & Cat, T., 1988. The Whittier Narrows, California, earthquake of October 1, 1987: CSMIP strong motion data, Earthquake Spectra, 4, 75-100.

Spudich, P., Hellweg, M., & Lee, W.H.K., 1996. Directional topographic site response at Tarzana observed in aftershocks of the 1994 Northridge, California, earthquake: implications for mainshock motions, Bull. seism. Soc. Am., 86, S193–S208.

Tucker, B. E., King, J. L., Hatzfeld, D., & Nersesov, I. L., 1984. Observations of hard rock site effects, Bull. seism. Soc. Am., 74, 121–136.

Turcotte, D.L., 1997. Fractals and chaos in geology and geophysics (2nd Edition), Cambridge University Press, Cambridge.

Vidale, J.E., 1986. Complex polarisation analysis of particle motion, Bull. seism. Soc. Am., 76, 1393–405.

Weiss, A., 2001. Topographic position and landforms analysis: Poster presentation, ESRI User Conference, San Diego, CA. (available online at http://www.jennessent.com/downloads/tpi-poster-tnc_18x22.pdf, last accessed: June 11, 2013).

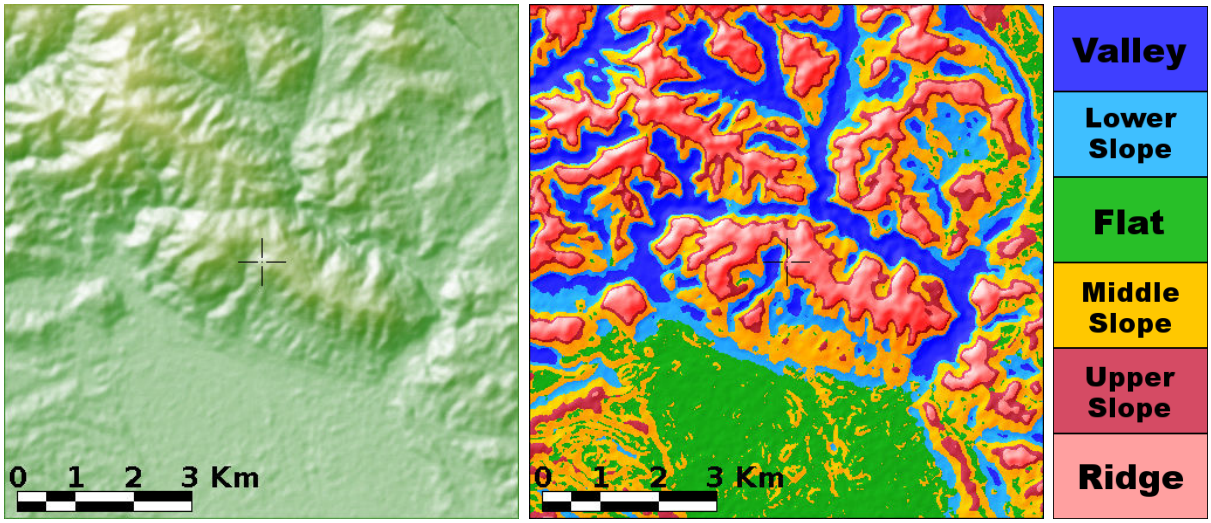

Figure 1: Digital elevation model (on the left) and slope classification (on the right). The black cross denotes the location of the seismic station. A spatial window of 1020 m was used in this example.

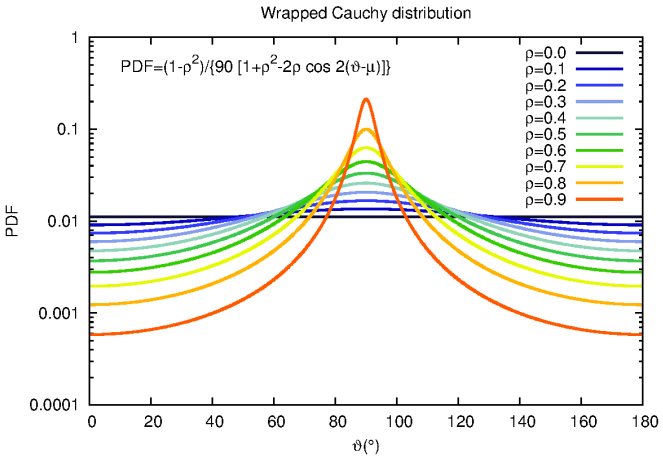

Figure 2: The Wrapped Cauchy distribution is used for the description of strike and dip angles. It is characterized by mean μ and concentration parameter ρ. The presented examples have all 180° period, mean μ=90° and show the influence of concentration ρ (different colors).

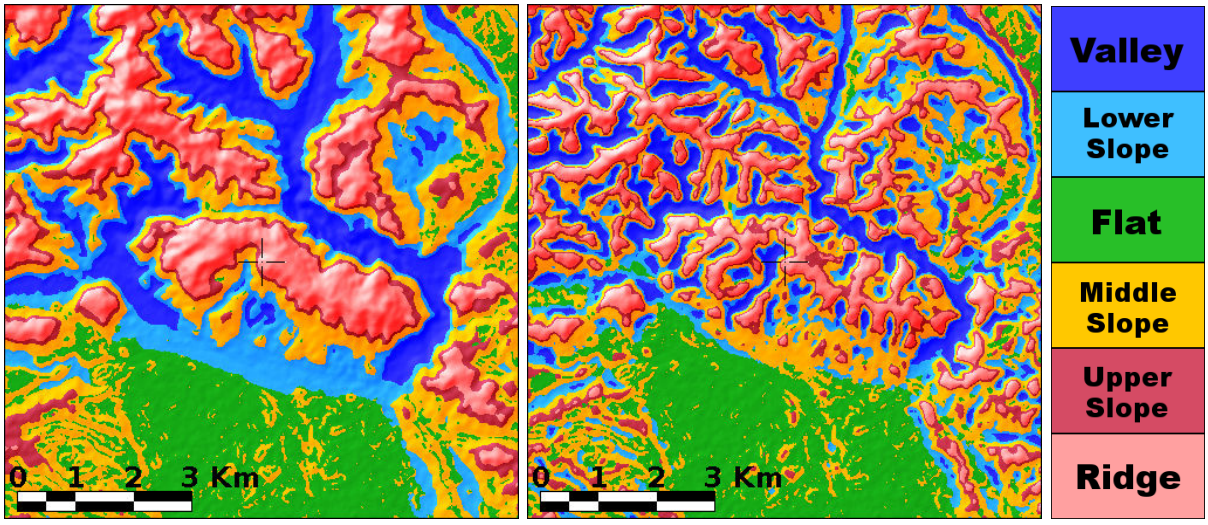

Figure 3: An example of the slope classification's dependence on the *scale*. Spatial windows of 2020 m (on left) and of 500 m (on right) were utilized in classification. The DEM is the same as in the Figure 1.

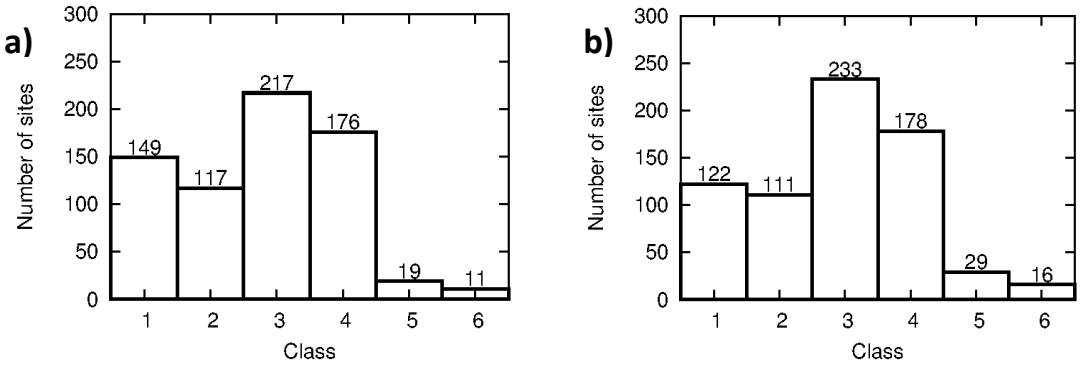

Figure 4: Distribution of the KiK-net sites according to terrain classes: a) at 1020 m scale; b) at 500 m scale. The definition of the classes is in the Table 1.

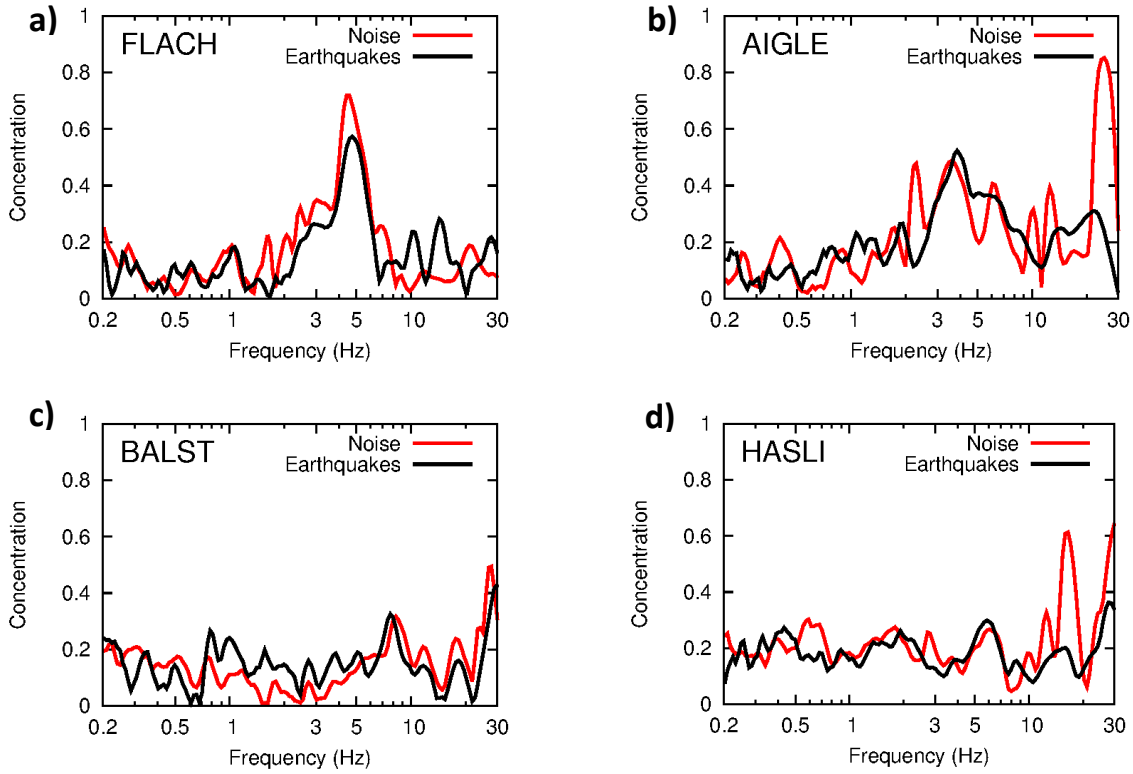

Figure 5: Concentrations of polarization strike angles as a function of frequency. Comparison of the polarization analysis for earthquakes and ambient vibrations – typical situations: a) a station with ground motion directionality and good agreement; b) a station with ground motion directionality and with peaks in the curve obtained from ambient vibrations caused by anthropic sources; c) a station without ground motion directionality and good agreement; d) a station with ground motion directionality and with peaks in the curve obtained from ambient vibrations caused by anthropic sources;

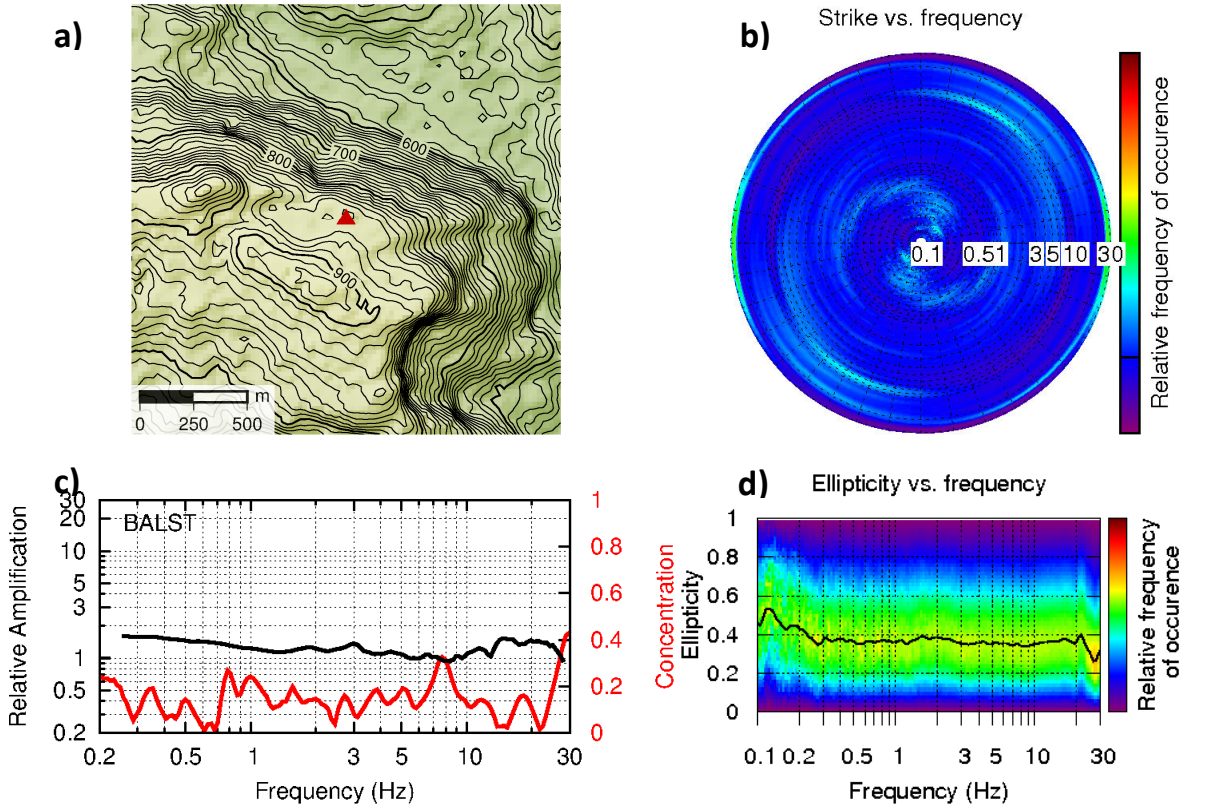

Figure 6: An example of a site with no site effect (Station BALST): a) geometry of the terrain (based on Swiss Topo LIDAR swissALTI3D DEM, contour lines placed for every 10 m) and location of the station (red triangle); b) distribution of the strike angle; c) concentration vs. amplification; d) distribution of the ellipticity.

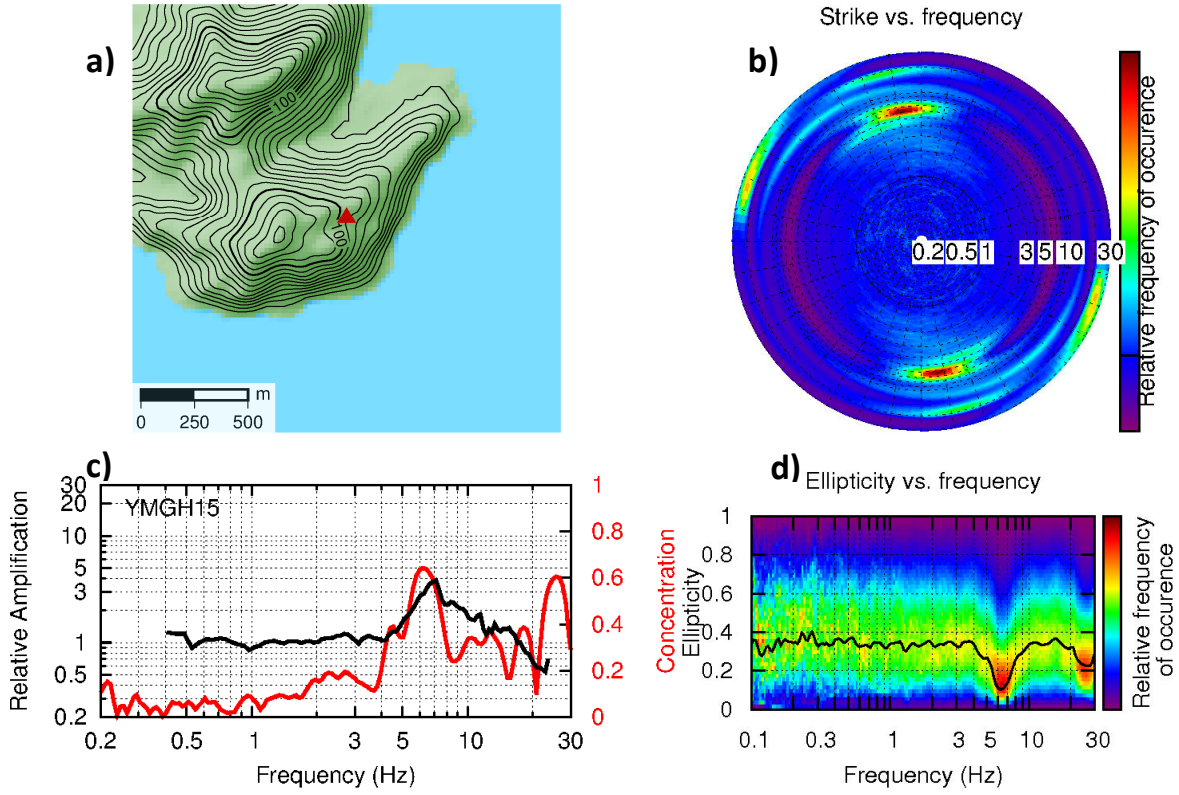

Figure 7: An example of a site with relatively strong site effect (Station YMGH15): a) geometry of the terrain (based on ASTER GDEM, contour lines placed for every 10 m) and location of the station (red triangle); b) distribution of the strike angle; c) concentration vs. amplification; d) distribution of the ellipticity.

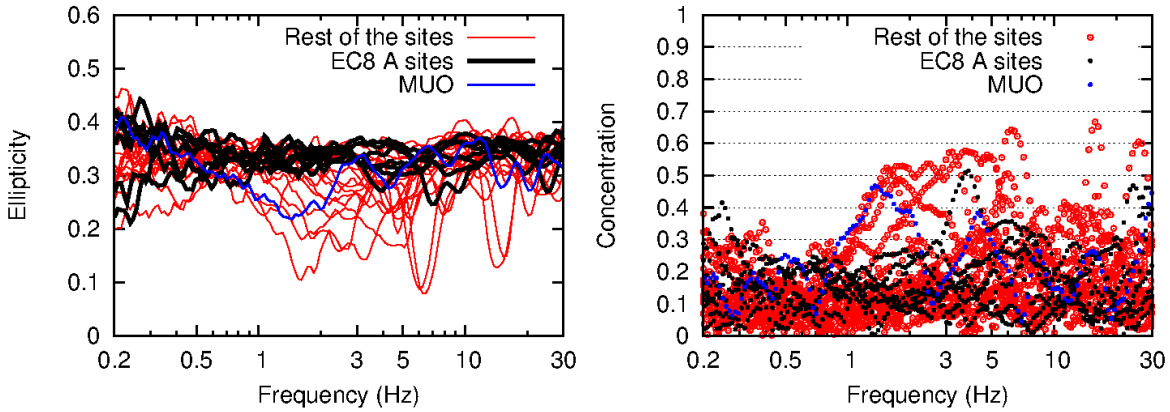

Figure 8: Comparison of the polarization analysis for station MUO (blue), EC8 class A stations (black) and rest of the stations (red) at KiK-net and Swiss sites. Modes of the ellipticity distributions are plotted on the left plot, whereas concentrations of the strike angle are on the right plot.

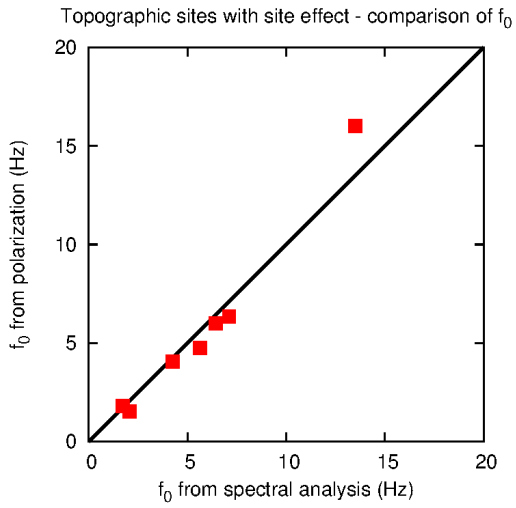

Figure 9: Fundamental frequencies picked from the amplification obtained from spectral fitting and from the polarization analysis. This assessment has been done for sites with clear directionality. The picks are presented in the Appendix (Appendix B of this document).

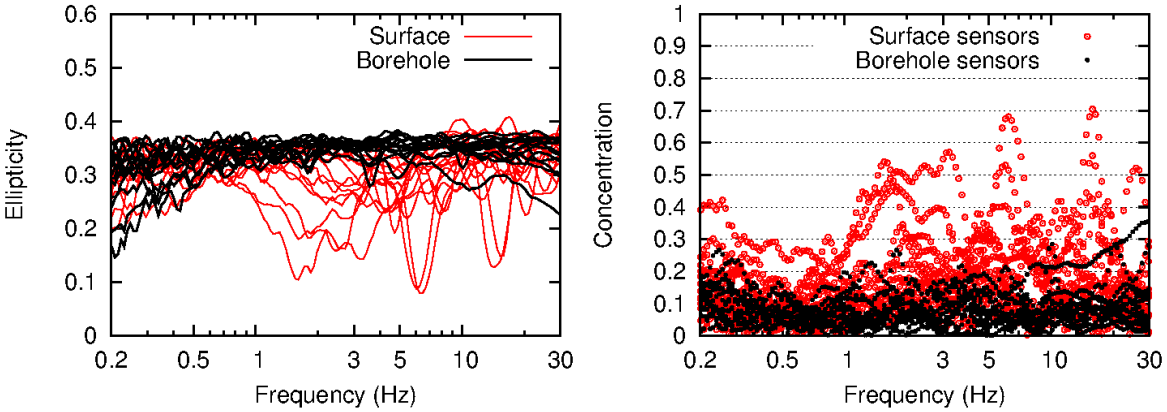

Figure 10: Comparison of the polarization analysis for surface (red) and borehole instruments (black) at KiK-net sites. Modes of the ellipticity distributions are plotted on the left plot, whereas concentrations of the strike angle are on the right plot.

Class number	Class name	TPI range	Slope
1	Valley	$TPI \leq -\sigma_{TPI}$	-
2	Lower Slope	$(-\sigma_{TPI}, -0.5\sigma_{TPI})$	-
3	Flat area	$(-0.5\sigma_{TPI}, 0.5\sigma_{TPI})$	Slope≤5°
4	Middle Slope	$(-0.5\sigma_{TPI}, 0.5\sigma_{TPI})$	Slope>5°
5	Upper Slope	$(0.5\sigma_{TPI}, \sigma_{TPI})$	-
6	Ridge	$TPI \geq \sigma_{TPI}$	-

Table 1: Terrain classification.

CODE	Borehole depth (m)	Vs100 (m/s)	Vs30 (m/s)	EC8 Class	f_0^{ampl} (Hz) / f_0^{pol} (Hz)	Lithology
AICH07	201	1001	428	B	-	Gravel and Sand (14m), Gneiss
NARH01	99	792	338	C	-	Slate
WKYH08	112	590	344	C	1.7 / 1.8	Hard weathered sandstone (27m), Sandstone
KMMH10	300	712	463	B	-	Talus deposit (11m), Sandstone, Shale
NGSH06	200	1803	1421	A	-	Strongly weathered green schist (7m),Schist
OITH10	100	1366	837	A	-	Clay (4m), Sandstone / Shale
MYGH09	100	560	358	C	13.5 / 16.0	Sand+Gravel(6m), Ash breccia and Curd / Silt
EHMH08	100	729	364	B	-	Gravel clay mixed (18m), Green and red shale rock
KGSH12	150	977	452	B	-	Aplite (25m), Granodiorite
YMGH15	110	1120	549	B	7.1 / 6.3	Weathered crystalline schist (16m), Sandy / Pelticschists
KNGH20	106	503	273	C	-	Soil (2m), Tuff, Conglomerate
SZOH34	118	699	430	B	6.4 / 6.0	Loam (13m), Lapilli tuff, Sandstone / Conglomerate / Basaltic rock
SZOH35	300	324	158	D	2.1 / 1.5	Sand and Gravel (13m), Rocks / Basaltic rock, Ash breccia and Curd
CHBH16	2003	542	361	B	-	Mudstone / Sandstone interbedded (140m)
ACB	-	-	658	B	-	Station in weathered rock (Jurassic sediments), about 10m below the surface. Surface material: gravels
AIGLE	-	-	1243	A	-	Station about 20m below the surface in rock: Jurassic (Malm) sediments ,limestones
BALST	-	-	1348	A	-	Rock: Jurassic (Malm) sediments,

						limestone with karst formations
FLACH	-	-	610	B	5.6 /4.8	Lower Freswater Molasse (USM, Aquitanien): layered sandstones, marl and conglomerates; Surface material: unconsolidated, loose scree.
HASLI	-	-	1603	A	-	Rock: Jurassic (Malm) sedimentshard, massive limestone
MUO	-	-	1086	A	-	Lower Cretaceous limestone
PLONS	-	-	1810	A	-	Permian sedimentary rock(Verrucano)
SLE	-	-	686	B	-	Mesozoic sediment ridge (limestone and marl)
STEIN	-	-	387	B	-	Rock composed of sediments of the Upper Freshwater Molasse (OSM, Miocene). Surface material: loose sediments.
SULZ	-	-	1028	A	-	Mesozoic sediment ridge (massive limestones)
WILA	-	-	683	B	4.2 /4.1	Unsorted conglomerates (Nagelfluh) (Upper Freshwater Molasse)

Table 2: Site characterization of the sites located on ridges. EC8 classification is based on Vs30 values. The colour of the field in the 6th column distinguishes the level of directionality: strong directionality (red), weak directionality (green), no directionality + no amplification (blue), not classified (white).

Appendix B

Digital elevation models, amplifications and polarization analysis of KiK-net and Swiss sites

SUPPORTIVE INFORMATION

Results for all sites analyzed in this study. 1st column: geometry of the terrain (based on ASTER GDEM, contour lines placed for every 20 m) and location of the station (red triangle). 2nd column: distribution of the strike angle. 3rd column: distribution of the ellipticity. 4th column: concentration vs. amplification. The vertical lines in amplification and concentration plots represent the corresponding picks of the fundamental frequencies.

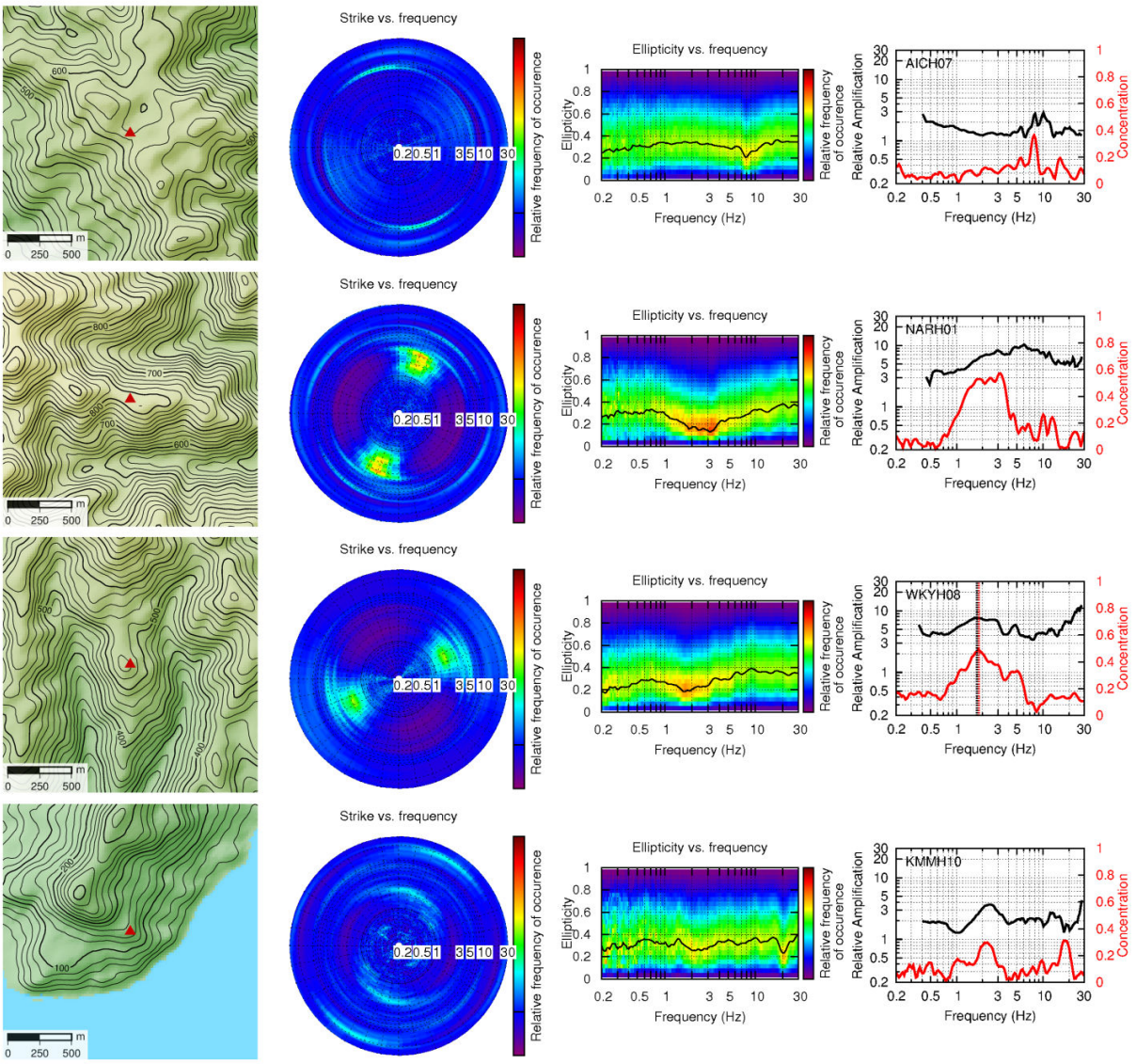

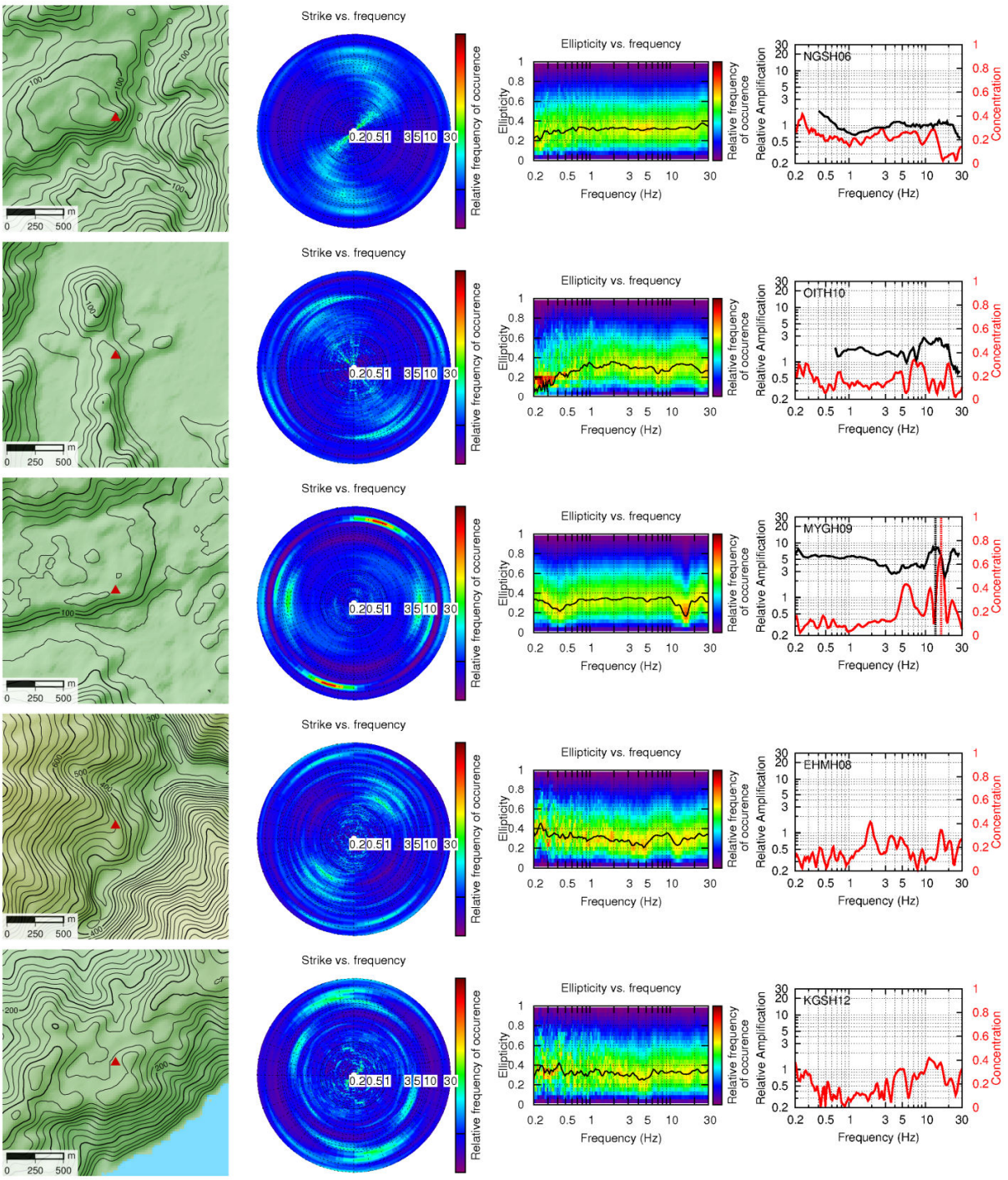
Strike vs. frequency
Relative frequency of occurence
Ellipticity vs. frequency
Ellipticity
Frequency (Hz)
Relative Amplification
Concentration
NGSH06
OITH10
MYGH09
EHMH08
KGSH12
0 250 500 m

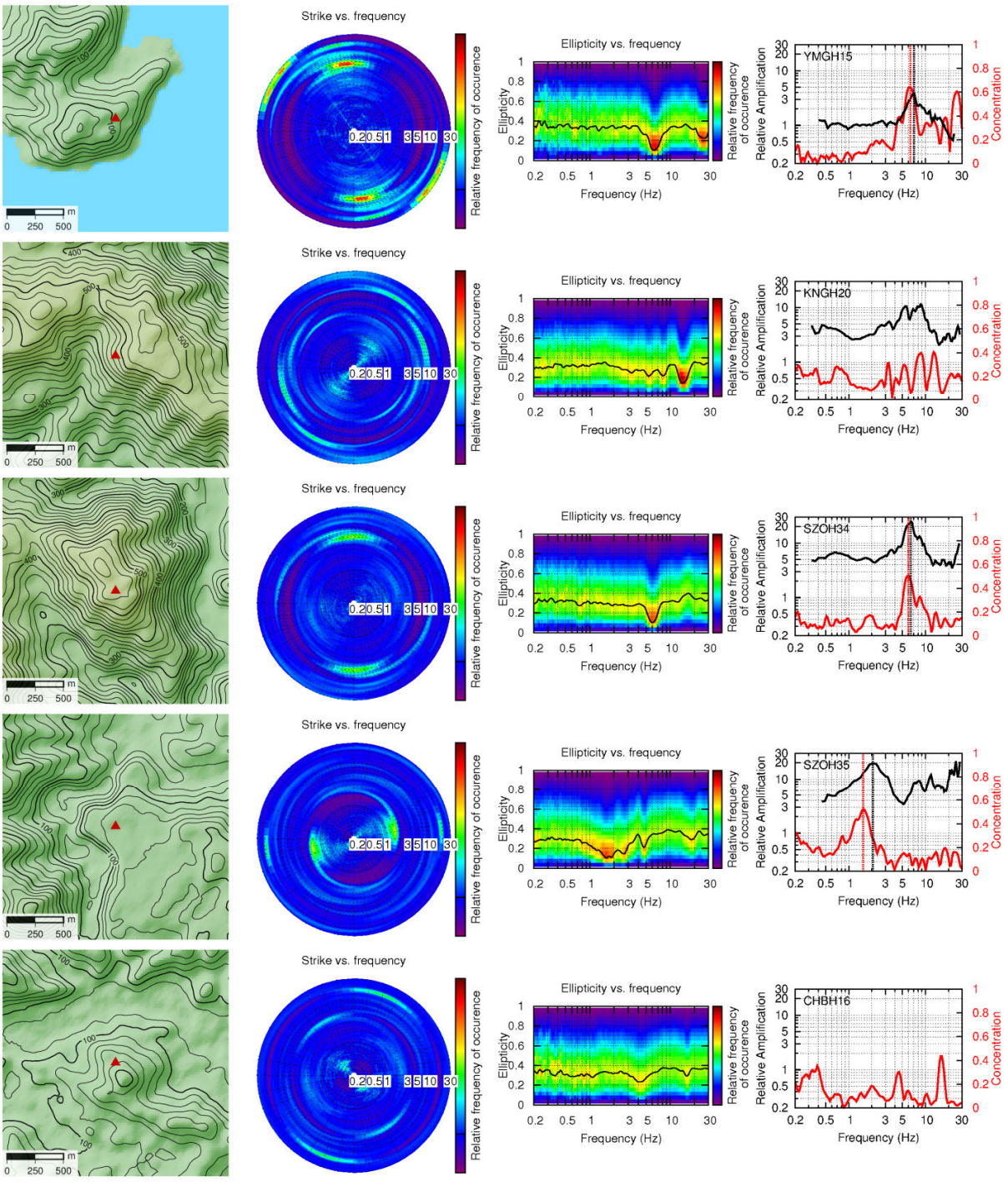
Strike vs. frequency
Relative frequency of occurence
Ellipticity vs. frequency
Ellipticity
Frequency (Hz)
Relative Amplification
Concentration
YMGH15
KNGH20
SZOH34
SZOH35
CHBH16
0 250 500 m

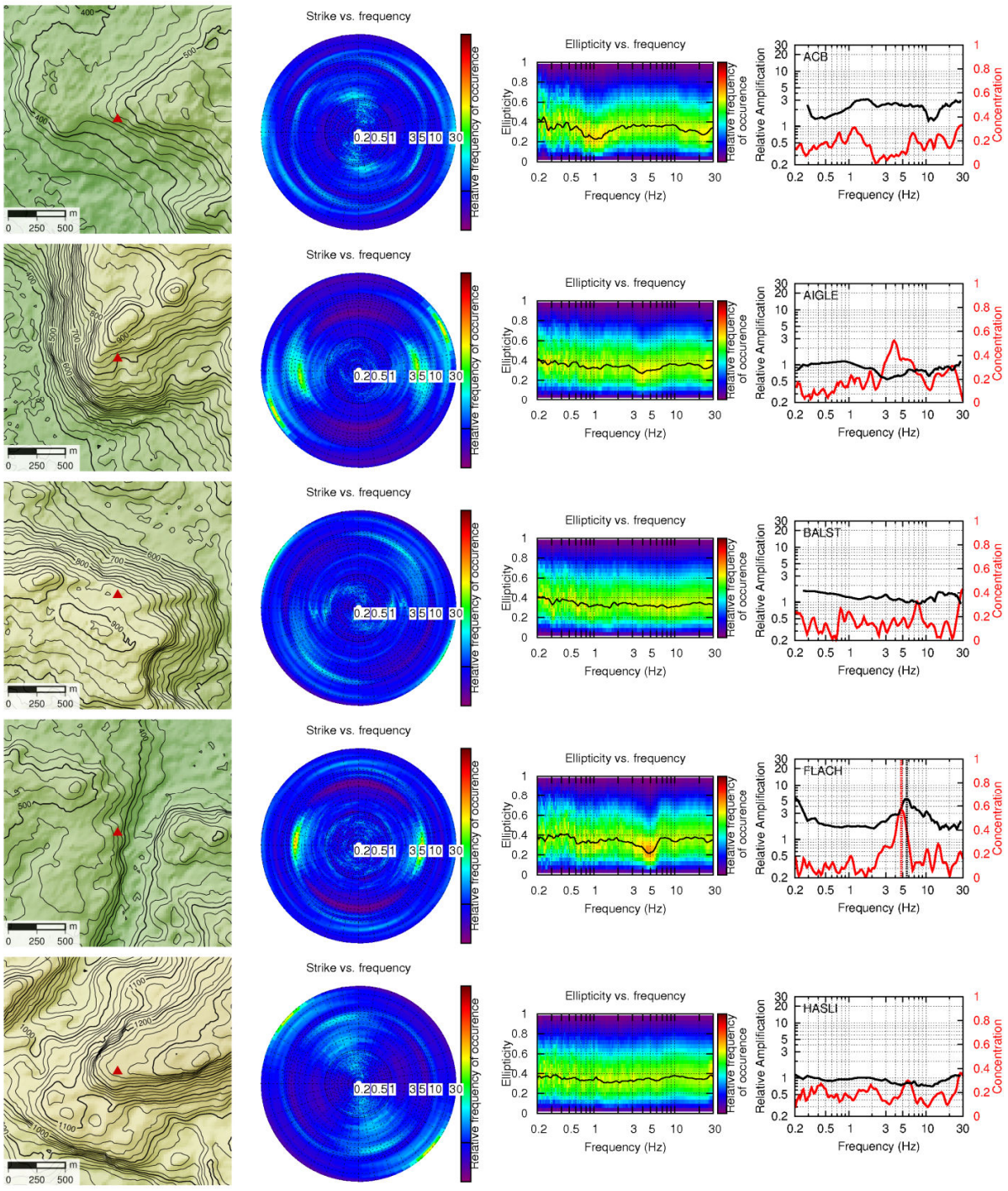
Strike vs. frequency
Relative frequency of occurence
0.2 0.5 1 3 5 10 30
Ellipticity vs. frequency
Ellipticity
Frequency (Hz)
Relative Amplification
Concentration
ACB
AIGLE
BALST
FLACH
HASLI
0 250 500 m

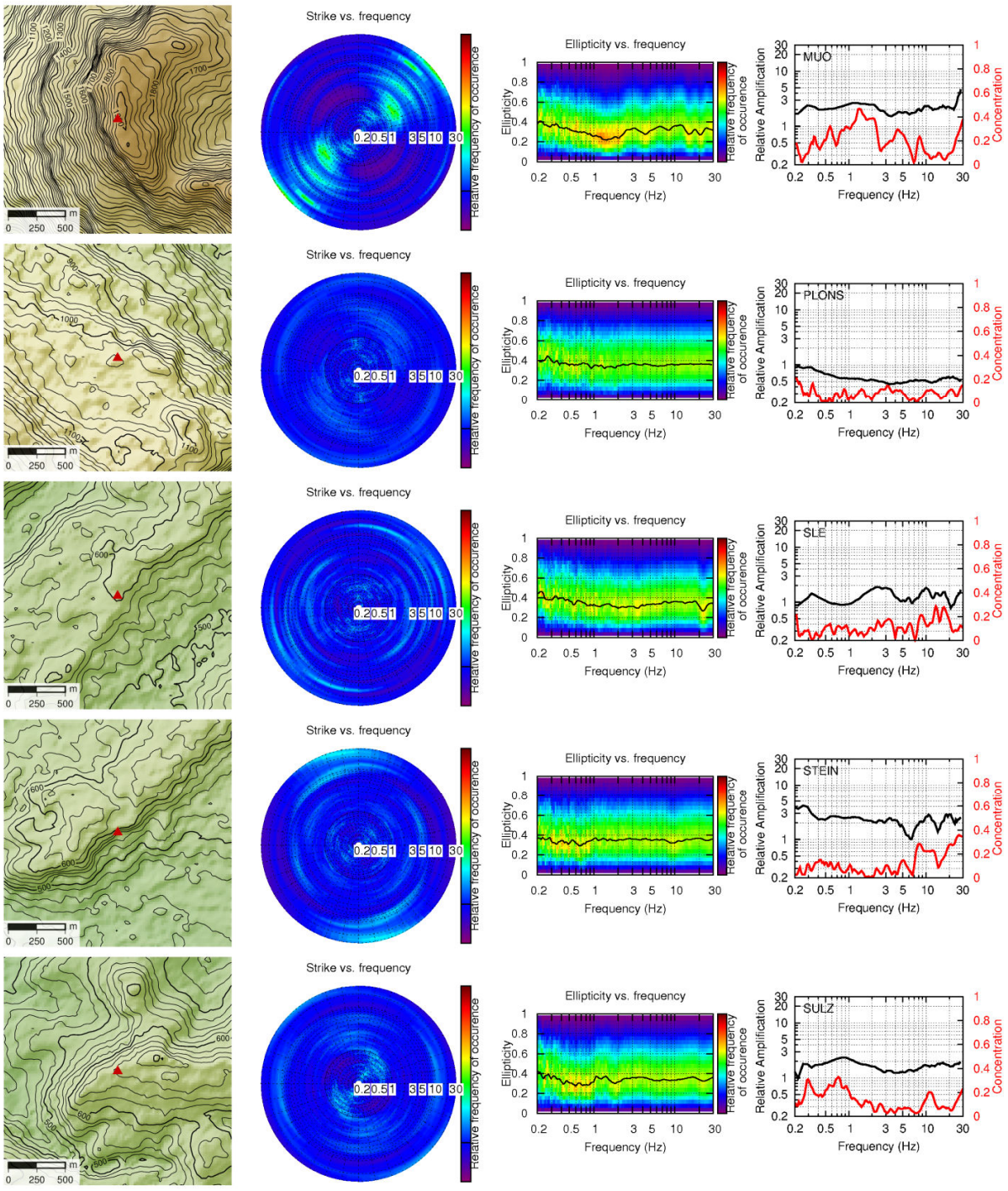
Strike vs. frequency
Ellipticity vs. frequency
Relative frequency of occurence
Ellipticity
Frequency (Hz)
Relative Amplification
Concentration
MUO
PLONS
SLE
STEIN
SULZ
0 250 500 m

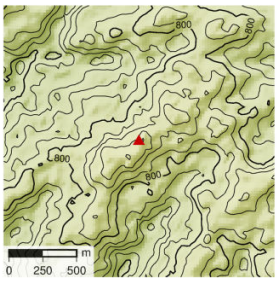
800
600
800
600
m
0 250 500

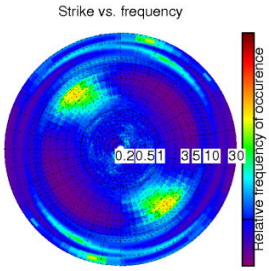
Strike vs. frequency
0.2 0.5 1 3 5 10 30
Relative frequency of occurence

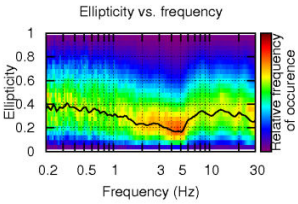
Ellipticity vs. frequency
Ellipticity
1
0.8
0.6
0.4
0.2
0
0.2 0.5 1 3 5 10 30
Frequency (Hz)
Relative frequency of occurence

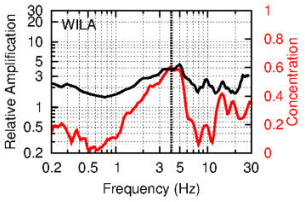
WILA
Relative Amplification
30
20
10
5
3
1
0.5
0.2
0.2 0.5 1 3 5 10 30
Frequency (Hz)
Concentration
1
0.8
0.6
0.4
0.2
0

Appendix C

Digital elevation models and polarization analysis of Italian sites

Results for Italian broad-band sites analyzed. 1st column: geometry of the terrain (based on ASTER GDEM, contour lines placed for every 20 m) and location of the station (red triangle). 2nd column: distribution of the strike angle (noise). 3rd column: distribution of the ellipticity (noise). 4th column: concentration (earthquakes vs. noise).

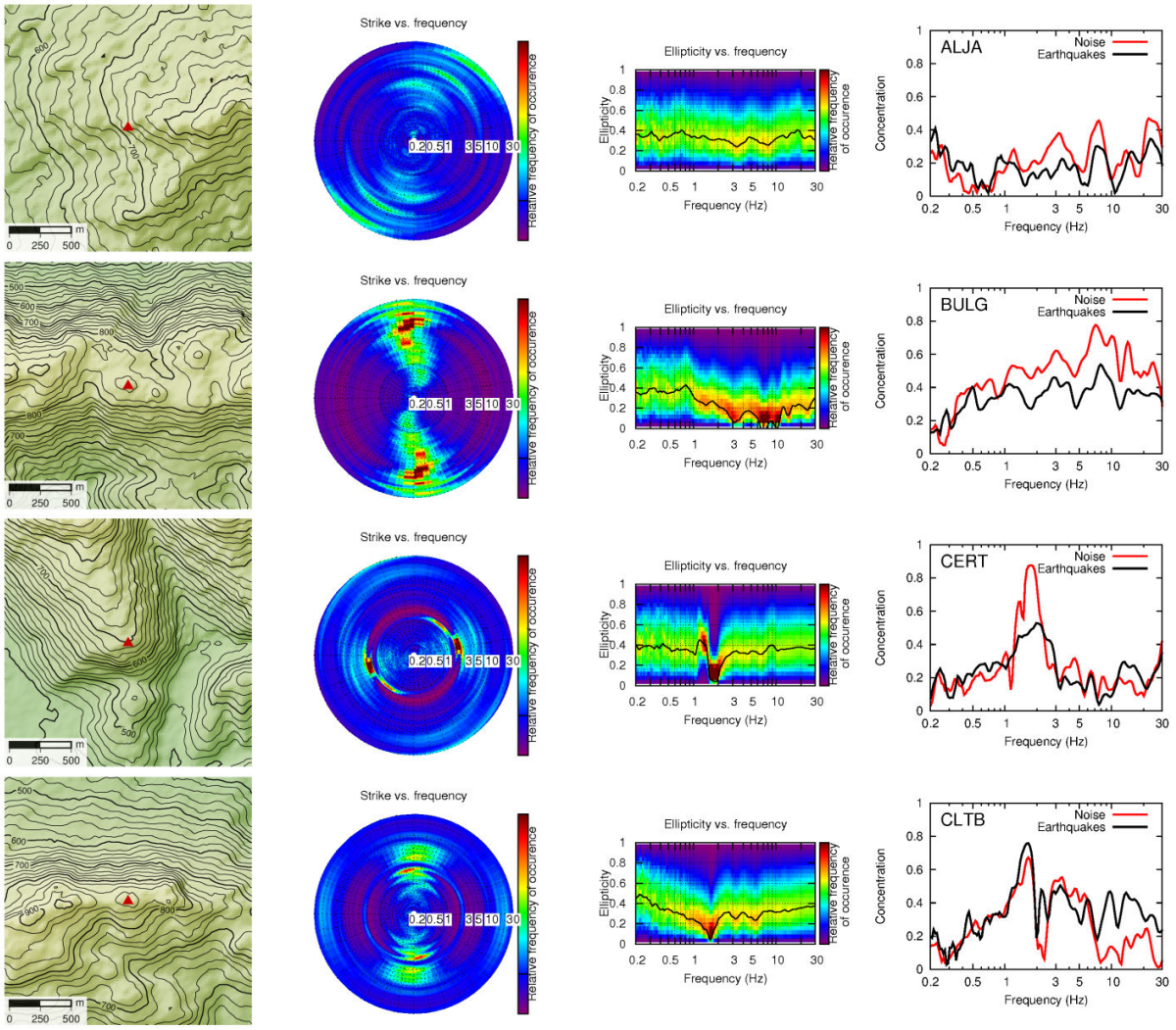

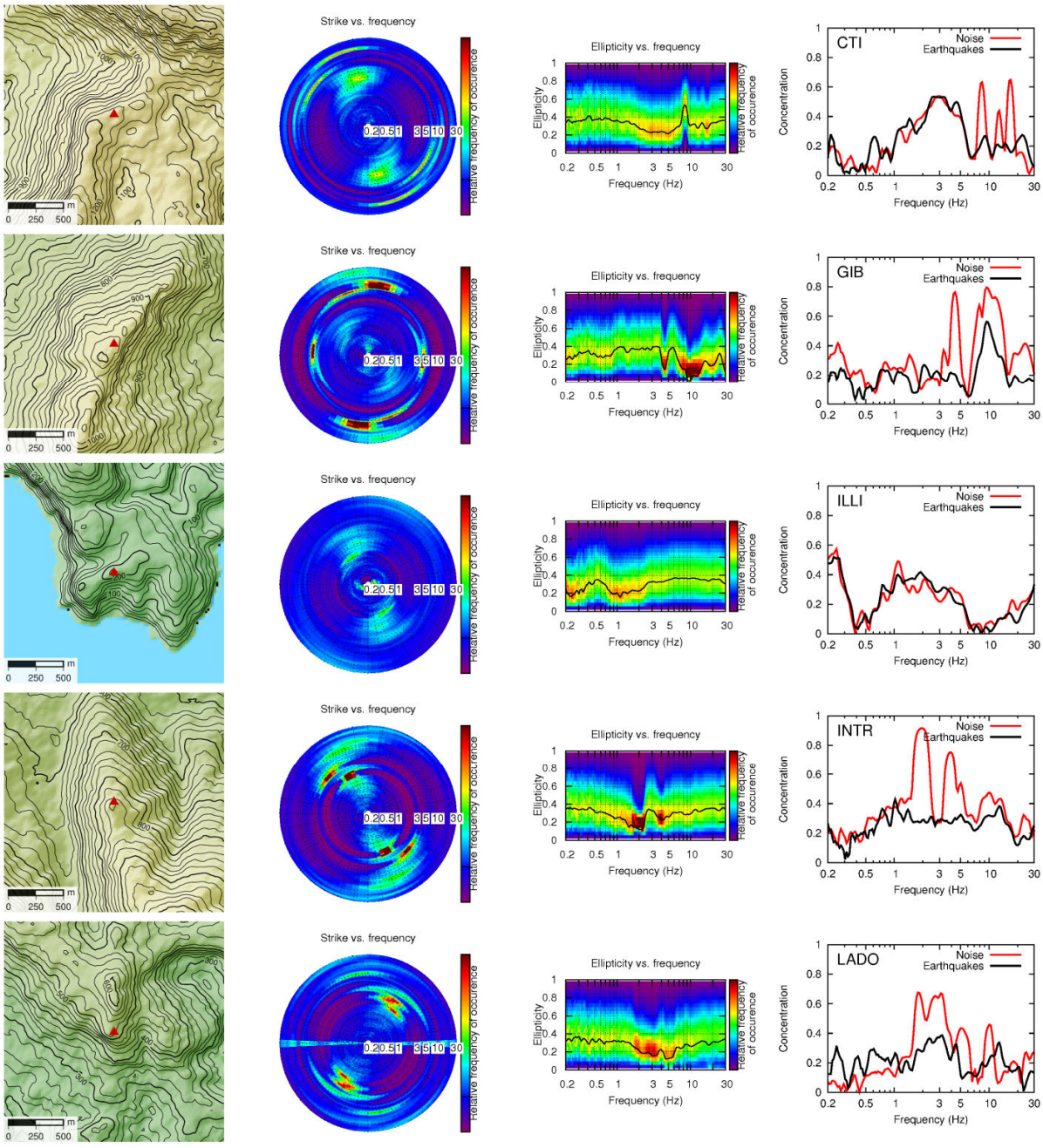
Strike vs. frequency
Relative frequency of occurence
0.2 0.5 1 3 5 10 30
Ellipticity vs. frequency
Ellipticity
Frequency (Hz)
CTI
GIB
ILLI
INTR
LADO
Noise
Earthquakes
Concentration
0 250 500 m

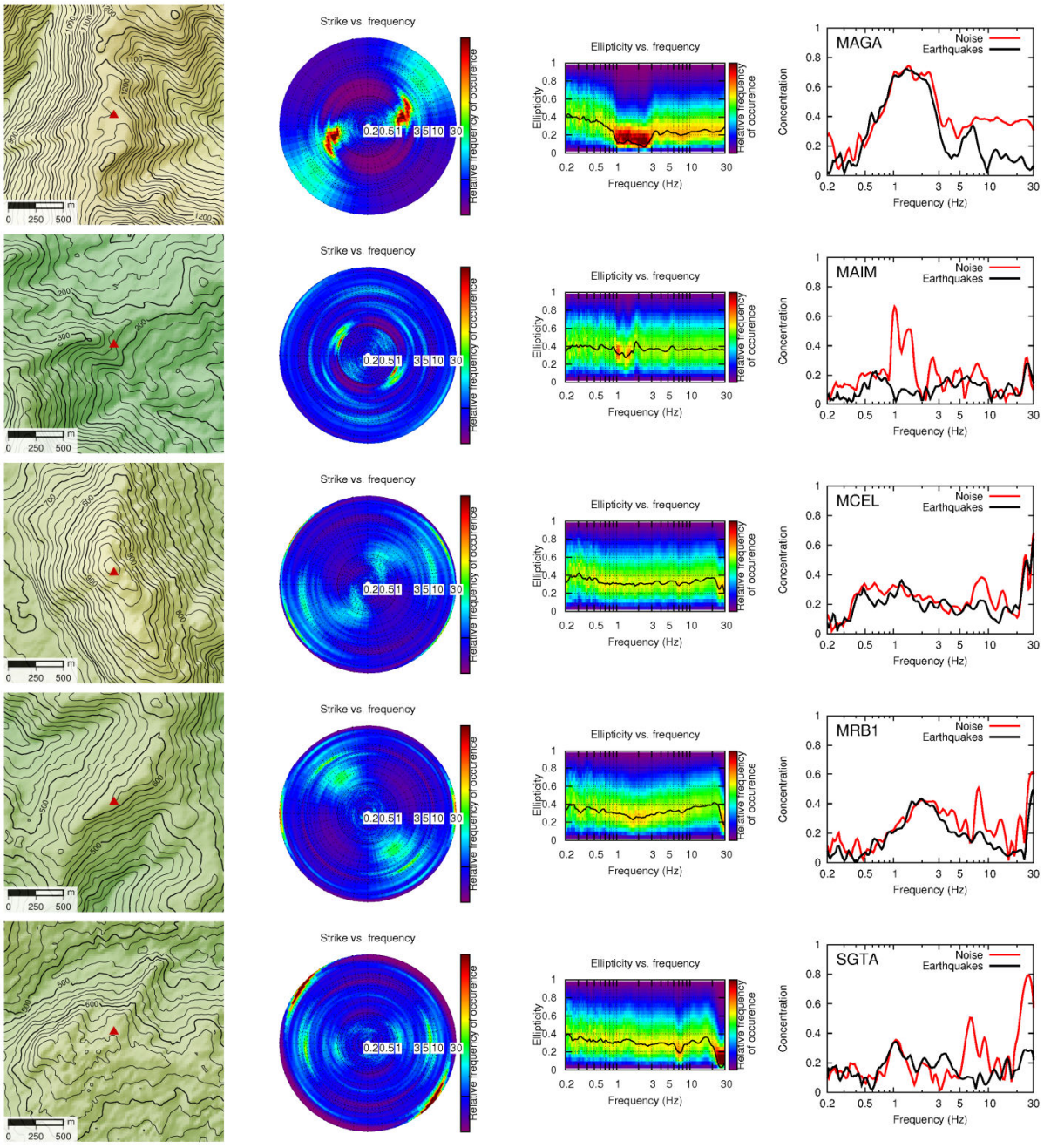
Strike vs. frequency
Ellipticity vs. frequency
Relative frequency of occurence
Ellipticity
Frequency (Hz)
Concentration
MAGA
MAIM
MCEL
MRB1
SGTA
Noise
Earthquakes
0 250 500 m

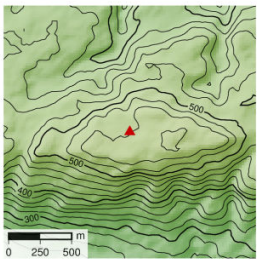
500
400
300
m
0 250 500

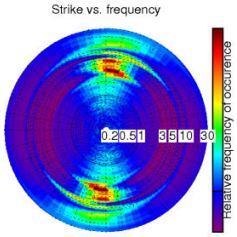
Strike vs. frequency
0.2 0.5 1 3 5 10 30
Relative frequency of occurence

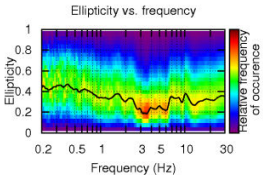
Ellipticity vs. frequency
Ellipticity
0 0.2 0.4 0.6 0.8 1
0.2 0.5 1 3 5 10 30
Frequency (Hz)
Relative frequency of occurence

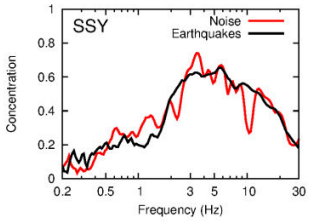
SSY
Noise
Earthquakes
Concentration
0 0.2 0.4 0.6 0.8 1
0.2 0.5 1 3 5 10 30
Frequency (Hz)

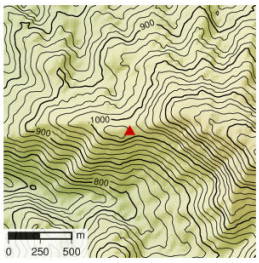
900
1000
900
800
m
0 250 500

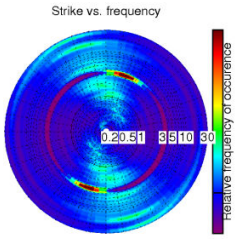
Strike vs. frequency
0.2 0.5 1 3 5 10 30
Relative frequency of occurence

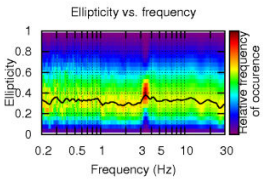
Ellipticity vs. frequency
Ellipticity
0 0.2 0.4 0.6 0.8 1
0.2 0.5 1 3 5 10 30
Frequency (Hz)
Relative frequency of occurence

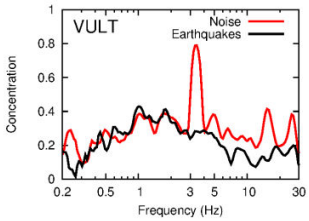
VULT
Noise
Earthquakes
Concentration
0 0.2 0.4 0.6 0.8 1
0.2 0.5 1 3 5 10 30
Frequency (Hz)

Appendix D

An overview of instrumented European sites with complex topography

Toward Reliable Characterization of Sites With Pronounced Topography and Related Effects on Ground Motion

J. Burjánek, C. Cauzzi & D. Fäh
Swiss Seismological Service, ETH Zürich, Zürich, Switzerland

P.-Y. Bard & C. Cornou
I nstitut des Sciences de la Terre (ISTerre), Grenoble, France

K. Pitilakis
Aristotle University of Thessaloniki, Thessaloniki, Greece

M. Massa
Istituto Nazionale di Geofisica e Vulcanologia, Milano, Italy

N. Theodulidis
Institute of Engineering Seismology and Earthquake Engineering, Thessaloniki, Greece

E. Bertrand
CETE Méditerranée, Nice, France

SUMMARY:
Here we present first results of a joint effort undertaken in ongoing European project NERA -JRA1, which aims at establishing scientifically solid and practically acceptable propositions to incorporate surface topography effects in seismic hazard estimates. We assembled a dataset of both ambient vibration and earthquake recordings acquired at 40 European sites with pronounced topography. It comprises a wide variety of sites including populated hills and even extreme cases of unstable rock slopes in Alpine regions. Results of the polarisation analysis for the two sites presented here show the peculiarity of the topographic site effects.

Keywords: Topographic site effects, Data mining, Site characterization

1. INTRODUCTION

The effects of surface topography geometry on seismic ground motion have been recognized for a long time, and have been the topic of many instrumental and numerical investigations over the last four decades. However, their complexity, combined with the limitations of both geophysical investigation techniques and numerical simulation, made it impossible till now to include such effects in earthquake hazard assessment and risk mitigation policies. In a number of cases, observed amplification cannot be explained only by the geometry of the topography, and is probably tightly linked also with local sub-surface structure (e.g., Spudich et al., 1996; Assimaki et al., 2005; Glinsky and Betrand, 2011). Moreover, topographic site effects are also usually linked to co-seismic landslides, which contribute significantly to earthquake damage. However, in case of unstable slopes, purely geometrical effects are almost negligible compared to the combined effect of the topography and subsurface structure (Moore et al., 2011).
Here we present first results of a joint effort undertaken in ongoing European project NERA -JRA1, which aims at establishing scientifically solid and practically acceptable propositions to incorporate surface topography effects in seismic hazard assasment. The key is a reasonable characterization of the both topographic site structures and observed effects on ground motion. Concerning the ground motion analysis, a number of studies found the topographic site effects to be directional (e.g., Bonamassa and Vidale 1991; Spudich et al. 1996; Del Gaudio and Wasowski, 2007; Burjanek et al. 2010; Pischiutta et al.,

2010 and 2011; Panzera et al., 2011, Burjanek et al., 2012). Thus we propose the polarization analysis of particle motion as an additional element of the ground motion characterization. We assembled a dataset of both ambient vibration and earthquake recordings acquired at 40 European sites with pronounced topography. It comprises a wide variety of sites including populated hills and even extreme cases of unstable rock slopes in Alpine regions. This dataset allows a systematic study with common processing tools, providing homogeneous results. The presumed ground motion attributes are sets of azimuthally dependent resonant frequencies, amplifications factors (e.g. with respect to widely used ground motion prediction equations), and near-surface attenuation (e.g. represented by kappa). Concerning structural description of the selected 40 sites, digital elevation models will be analyzed, together with available velocity profiles. A special attention will be paid to reasonable characterization of near-surface rock fracturing and weathering, which generate amplification at presumable rock sites. A systematic comparison of the proposed ground motion and structural attributes should allow the rational classification of the topographic sites, which would further improve the general quantification of the related site effects (e.g. through the numerical simulations). In this paper we present just preliminary results, illustrating mainly the motivation for the study.

2. AVAILABLE DATA

A number of instrumented sites suitable for studying potential topographic effects were identified in Italy, Switzerland, Greece, and France (Fig 2.1). The available data are listed in Tab. 2.1. The sites are located either close to the top of hills and ridges or just in the middle of the slope. Both earthquake (weak motion) and ambient vibrations recordings were collected. The backbone of the dataset consists of the Italian and Swiss permanent seismic stations. Ground motion prediction equations will serve as a reference ground motion for these sites. Most of the Swiss permanent stations have a detailed site characterization including mean velocity profiles down to 30 m, and mean amplification functions relative to the Swiss reference profile (Fäh et al., 2009; Poggi et al., 2011). The rest of the locations are specific experiments related to the local site effects, thus a more detailed geophysical information is available for these sites. Nevertheless, these sites represent mostly extreme cases of the topography-related site effects (e.g., unstable rockslopes in Switzerland).

Table 2.1

	Permanent/Semi-permanent stations				Noise survey	
Site name	Ambient Vibration	Earthquake recordings	Number of stations	Reference station	Arrays	Single station
Italian BB stations	YES	YES	21	GMPE	NO	NO
Swiss BB stations	YES	YES	11	GMPE	2	NO
Aegion	NO	YES	1	YES	1	7
Grevena	YES	YES	1	YES	NO	NO
Narni Hill	YES	YES	10	YES	NO	YES
Nocera Umbra	NO	YES	6	YES	NO	YES
Castelvecchio Subequo	YES	YES	3	YES	NO	YES
Obervaz	YES	YES	1	NO	1	NO
Graechen	YES	YES	3	YES	3	30
Randa	YES	YES	1	YES	3	NO
Walkerschmatt	NO	NO	0	NO	3	NO
Rognes	YES	YES	9	YES	1	YES
Nice	YES	YES	5	YES	NO	YES

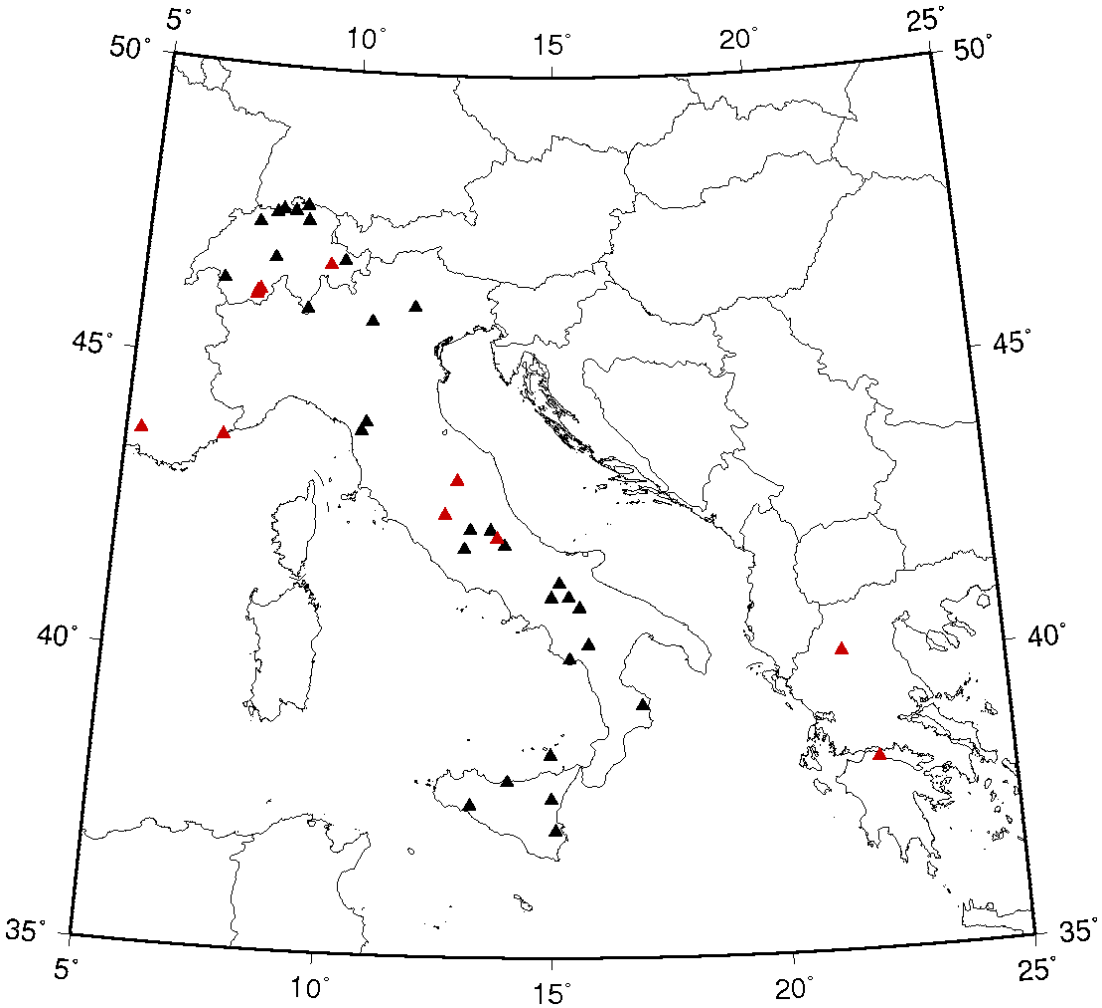

Figure 2.1: Overview of the sites included in the dataset (black: permanent broad-band instruments; red: additional sites with observed topographic site effects).

3. METHODS

Several methods exist for the analysis of the directional site effects. Spudich et al. (1996) introduced directional site-to-reference spectral ratios (SRSR) for the estimation of the relative amplification depending on both frequency and azimuth. This method has been widely applied (e.g., Pischiutta et al., 2010; Massa et al., 2010), however, it requires a reference station, which is not always available. Therefore, a directional non-reference H/V spectral ratio (HVSR) has been also applied (Del Gaudio and Wasowski, 2007). Whereas HVSR has been commonly applied on both earthquake and noise recordings, SRSR has been primarily used with earthquake recordings. Nevertheless, SRSR can be applied also on noise recordings, if it is assured, that the noise generating sources (for frequencies of interest) are far from the site (Roten et al., 2006; Burjanek et al., 2012). In this work, we have focused on the non-reference methods, as the reference is not available for most of the sites.

Recently, Burjanek et al. (2010) introduced time-frequency polarization analysis (TFPA), which is based on the combination of complex polarization analysis (Vidale, 1986) and the continuous wavelet transform (CWT). It can be viewed as a generalization of the directional HVSR method. Three polarization parameters are retrieved: 1) azimuth of the major axis, or strike, measured in degrees from North; 2) tilt of

the major axis, or dip, measured in degrees downward from the horizontal; and 3) ellipticity, defined as the ratio between the length of the semi-minor and semi-major axes. All three polarization parameters vary with both time and frequency. Usually, we assume that observed ambient vibrations are quasi-stationary (i.e. noise properties do not change systematically on the time scale of

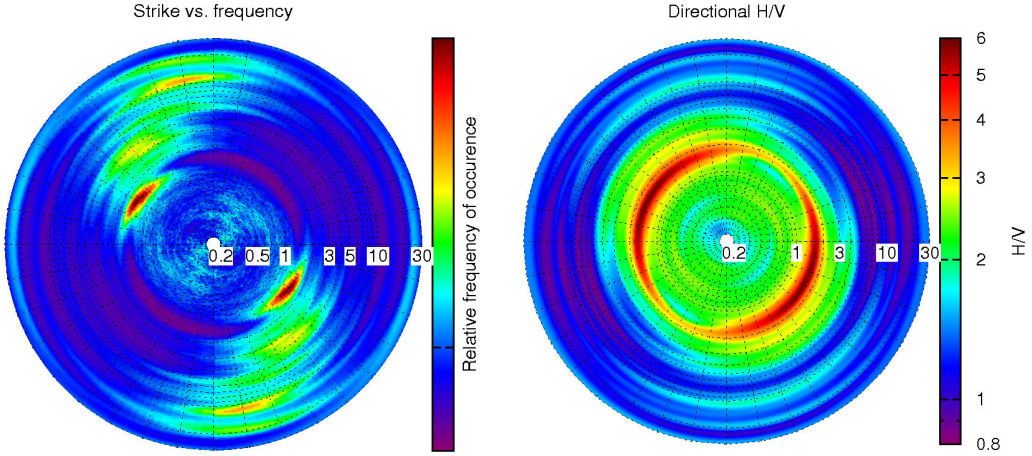

Figure 3.1: Comparison of two processing methods of single station three-component ambient vibration measurements. The relative occurrence of strike (azimuth) of ambient vibrations obtained with time-frequency polarization analysis is presented at left. The directional dependent H/V ratio is presented on right. Frequency changes along the radius from 0.2 to 30 Hz as indicated.

the experiment – a few hours), and analyze the relative occurrence of polarization parameters. In particular, histograms of polarization parameters are constructed over time for each frequency. Polar plots are then adopted for the presentation of final results, which illustrate combined angular and frequency dependence. As the directional HVSR can be used to estimate just the polarization azimuth (orientation in horizontal plane), TFPA method provides also information on the inclination of the particle motion (dip). Moreover, the use of CWT maintains optimum time-frequency resolution, which can be smoothly regulated by an adjustment of the mother wavelet. An example of the direct comparison of the directional HVSR and relative occurrence of azimuth (strike) obtained with TFPA for a common recording of ambient vibrations is presented in Fig. 3.1. TFPA clearly outperforms directional H/V providing better directional resolution.

4. PRELIMINARY RESULTS

Here we present a result of the polarization analysis using TFPA for two stations of the Swiss network. These two stations were selected as they represent two end cases (strong directional site effect vs. no directional site effect).

At first we present results for the station FLACH, which is located in the middle of the slope (Fig 4.1a). The site is instrumented with three component velocity sensor with an Eigen-period of 5 sec. Two hours of ambient vibration recording were processed. The results of TFPA are presented in Fig. 4.1. Note the drop of the ellipticity at the frequency of 4 Hz (particle motion is almost linear for most of the time). Moreover, strike (azimuth) concentrates around 95° for the same frequency (4 Hz). The observed direction (95°) is transversal to the topography elongation. An analysis of 9 earthquake recordings was also performed. Results are presented in Fig. 4.2. Generally, similar pattern is observed as for the ambient vibrations, just the minimum of the ellipticity is shifted to 5 Hz. Nevertheless, this might be related to the relatively low number of available earthquake recordings. To conclude, site FLACH presents a typical example of the directional site effect.

At second, we present results for the station BALST, which is located just on the cliff (Fig. 4.3a), where a strong topographic site effect is expected. The site is instrumented with three component velocity sensor with an Eigen-period of 120 sec. Two hours of ambient vibration recording were processed. The results of TFPA are presented in Fig. 4.3. No specific polarization pattern is observed, apart from high-frequency disturbance, which is probably related to a local human activity. An analysis of 17 earthquake recordings was also performed. Results are presented in Fig. 4.4. Similarly to ambient noise recordings, no specific polarization pattern is observed. Concluding, site BALST does not present any strong directional site effect.

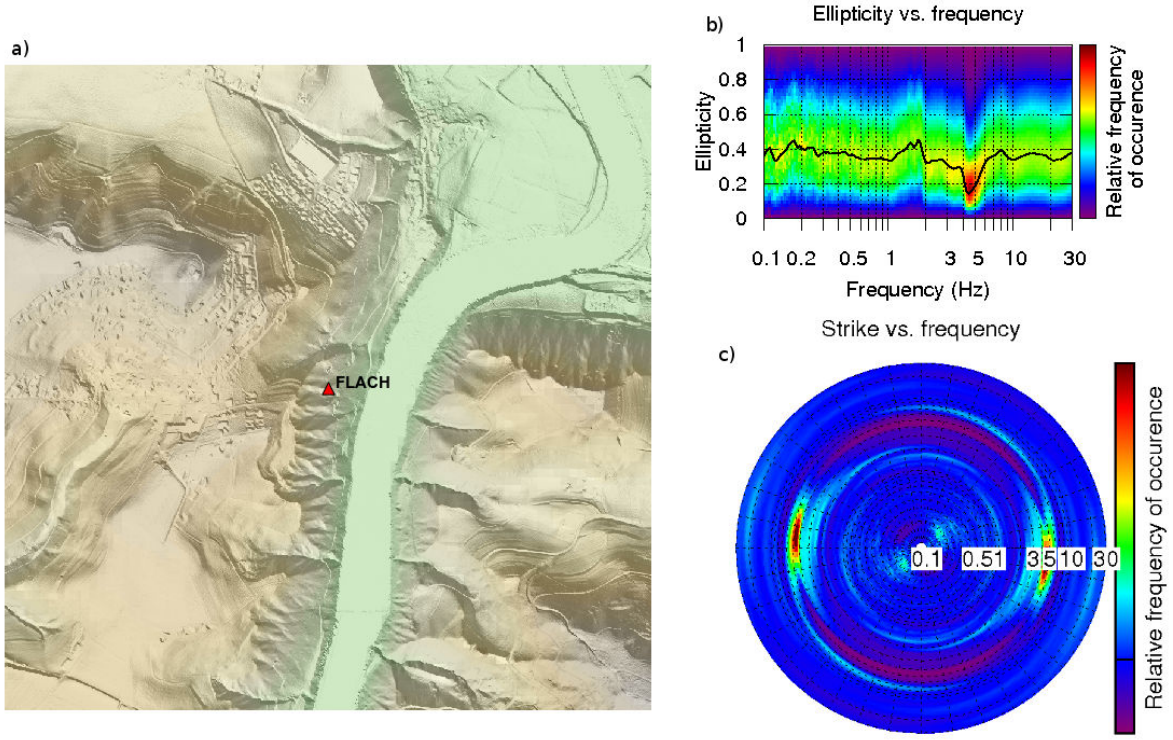

Figure 4.1: a) Site FLACH (+ surrounding area of 2 km x 2 km), the height of the ridge is approximately 150 m. b) Relative frequency of occurrence of ellipticity in ambient vibrations retrieved by TFPA. The mode of the ellipticity distribution is interconnected with the black line; c) Relative frequency of occurrence of strike in ambient vibrations retrieved by TFPA.

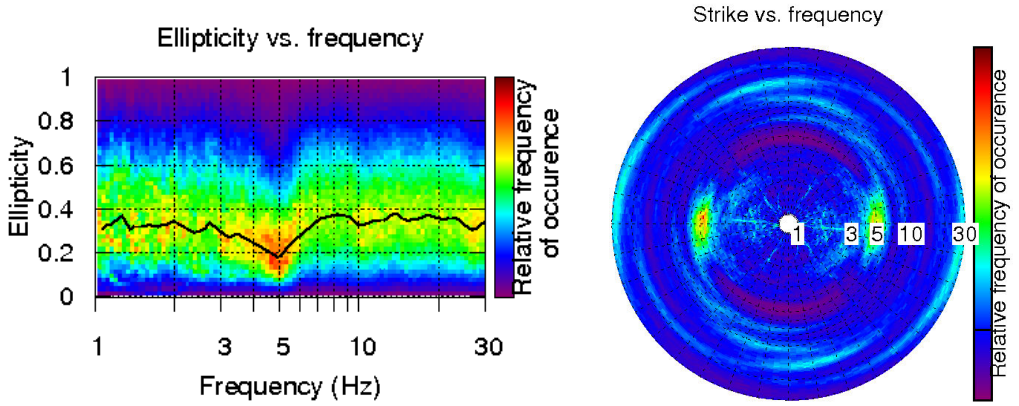

Figure 4.2: TFPA analysis of earthquake recordings at station FLACH: ellipticity distribution (on left) and strike distribution (on right).

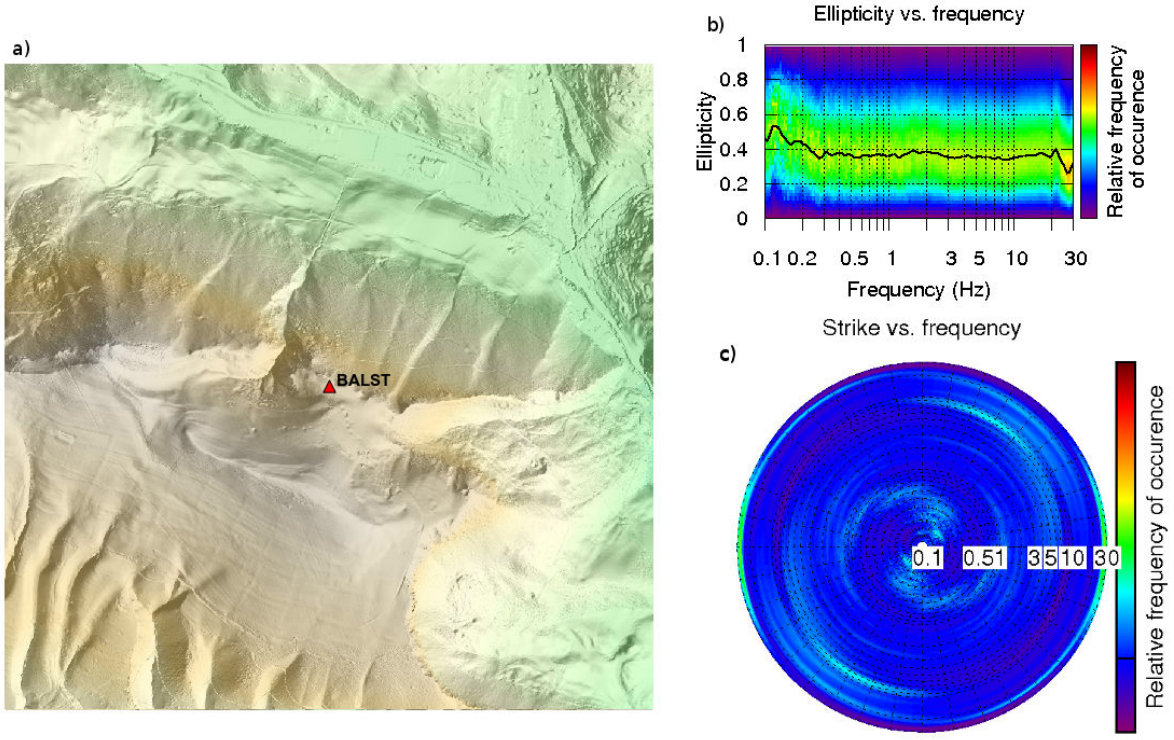

Figure 4.3: a) Site BALST (+ surrounding area of 2 km x 2 km), the height of the ridge is approximately 300 m. b) Relative frequency of occurrence of ellipticity in ambient vibrations retrieved by TFPA. The mode of the ellipticity distribution is interconnected with the black line; c) Relative frequency of occurrence of strike in ambient vibrations retrieved by TFPA.

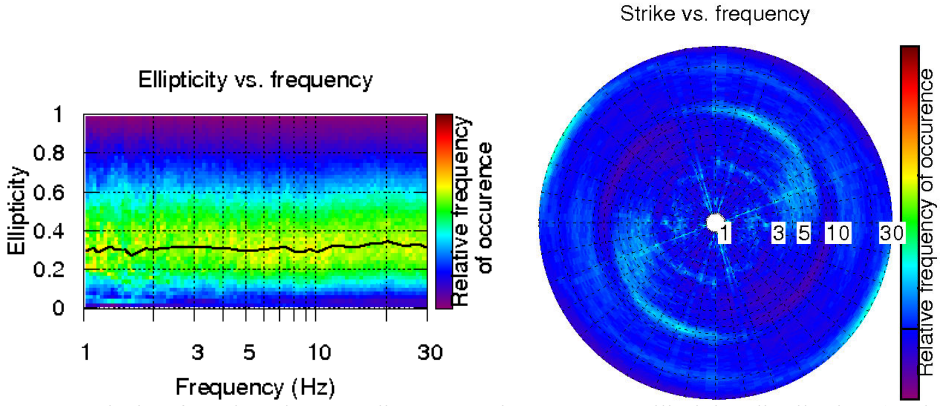

Figure 4.4: TFPA analysis of earthquake recordings at station BALST: ellipticity distribution (on left) and strike distribution (on right).

5. CONCLUSIONS AND OUTLOOK

The two sites presented here, show the peculiarity of the topographic site effects. Average residuals with respect to Swiss ground motion prediction model (GMPE) were also calculated for the two stations (Edwards, personal communication), and confirm the results presented here – station FLACH shows a

mean amplification of 5 at 5 Hz with respect to the Swiss reference profile (Poggi et al., 2011), whereas station BALST does not show any amplification at specific frequency based on the data used herein.
The project NERA is now in its second year. The work on topographic site effects has started in summer 2011, and conclusive results are expected after processing of the complete dataset. Moreover, set of new geophysical experiments is planned at selected sites in the framework of the project, and will help with the interpretation of the available station recordings.

AKCNOWLEDGEMENT
This research is part of the EU project NERA (Network of European Research Infrastructures for Earthquake Risk Assessment and Mitigation, task JRA1 – 'Waveform modelling and site coefficients for basin response and topography'). Wavelet software was provided by C. Torrence and G. Compo, available at http://paos.colorado.edu/research/wavelets/. Some figures in this paper were made using Generic Mapping Tools (GMT) 4 by Wessel & Smith (1998).

REFERENCES

Assimaki,D., Gazetas,G., and Kausel, E., (2005). Effects of local soil conditions on the topographic aggravation of seismic motion: parametric investigation and recorded field evidence from the 1999 Athens earthquake, *Bull. Seism. Soc. Am.*, **95:3**, 1059–1089.

Bonamassa, O. and Vidale, J.E., (1991). Directional site resonances observed from aftershocks of the 18th October 1989 Loma Prieta earthquake, *Bull. Seism. Soc. Am.*, **81**, 1945–1957.

Burjánek, J., Gassner-Stamm, G., Poggi, V., Moore, J. R., Fäh, D. (2010). Ambient vibration analysis of an unstable mountain slope, *Geophys. J. Int.*, **180:2**, 820-828.

Burjánek, J., J.R. Moore, G. Gassner-Stamm, and D. Fäh (2011). Seismic response of unstable mountain rock slopes: Topographic site effect?. *4th IASPEI / IAEE International Symposium: Effects of Surface Geology on Seismic Motion*, In CD. University of California Santa Barbara, CA, USA.

Burjánek, J., Moore, J.R., Yugsi-Molina, F.X., Fäh, D. (2012). Instrumental evidence of normal mode rock slope vibration, *Geophys. J. Int.*, **188:2**, 559-569.

Del Gaudio, V., and J. Wasowski (2007). Directivity of slope dynamic response to seismic shaking, *Geophys. Res. Lett.*, **34**, L12301.

Fäh, D., S. Fritsche, V. Poggi, G. Gassner-Stamm, P. Kästli, J. Burjanek, P. Zweifel, S. Barman, J. Clinton, L. Keller, P. Renault and S. Heuberger (2009). Determination of Site Information for Seismic Stations in Switzerland, Swiss Seismological Service Technical Report: SED/PRP/R/004/20090831, for the swissnuclear Pegasos Refinement Project.

Glinsky, N., and Bertrand, E. (2011). Numerical study of topographical site effects by a discontinuous finite element method. *4th IASPEI / IAEE International Symposium: Effects of Surface Geology on Seismic Motion*, In CD. University of California Santa Barbara, CA, USA.

Massa M., Lovati S., D'Alema E., Ferretti G. and Bakavoli M. (2010). An experimental approach for estimating seismic amplification effects at the top of a ridge, and the implication for ground-motion predictions: the case of Narni (central Italy), *Bull. Seism. Soc. Am.*, **100:6**, 3020-3034.

Moore, J.R., Gischig, V., Burjánek, J., Loew, S., Fäh, D. (2011). Site effects in unstable rock slopes: dynamic behavior of the Randa instability (Switzerland), *Bull. Seism. Soc. Am.*, **101:6**, 3110-3116.

Panzera, F., G. Lombardo, and R. Rigano (2011). Evidence of Topographic Effects through the Analysis of Ambient Noise Measurements, *Seism. Res. Lett.*, **82**, 413-419.

Pischiutta, M., G. Cultrera, A. Caserta, L. Luzi, and A. Rovelli (2010). Topographic effects on the hill of Nocera Umbra, central Italy, *Geophys. J. Int.*, **182**, 977–987.

Pischiutta, M., A. Rovelli, P. Vannoli, and G. Calderoni (2011). Recurrence of horizontal amplification at rock sites: a test using H/V based ground motion prediction equations. *4th IASPEI / IAEE International Symposium: Effects of Surface Geology on Seismic Motion*, In CD. University of California Santa Barbara, CA, USA.

Poggi, V., B. Edwards, and D. Fäh (2011). Derivation of a Reference Shear-Wave Velocity Model from Empirical Site Amplification, *Bull. Seism. Soc. Am.*, **101:1**, 258-274.

Roten, D., C. Cornou, D. Fäh, and D. Giardini (2006). 2D resonances in Alpine valleys identified from ambient vibration wavefields, *Geophys. J. Int.*, **165**, 889–905.

Spudich, P., Hellweg, M. & Lee, W.H.K., (1996). Directional topographic site response at Tarzana observed in

aftershocks of the 1994 Northridge, California, earthquake: implications for mainshock motions, *Bull. seism. Soc. Am.*, **86**, S193–S208.
Vidale, J.E., (1986). Complex polarisation analysis of particle motion, *Bull. Seism. Soc. Am.*, **76**, 1393–405.
Wessel, P., and W. H. F. Smith (1998). New, improved version of the Generic Mapping Tools released, *EOS Trans. AGU*, **79**, 579.

Appendix E

Polarization analysis for a typical 1D site

An example of polarization analysis for an approximately 1D KiK-NET site.

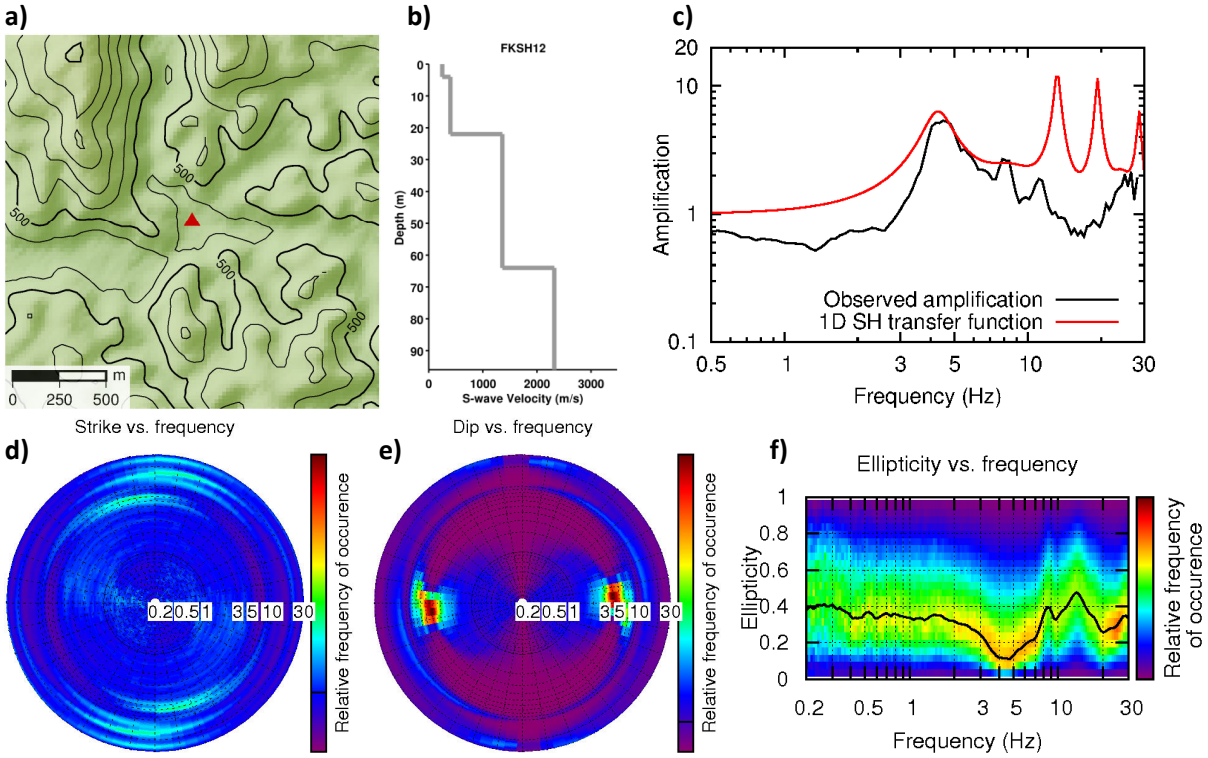

Figure 1: a) geometry of the terrain (based on ASTER GDEM, contour lines placed for every 20 m) and location of the station (red triangle); **b)** shear wave velocity profile; **c)** observed amplification function and 1D SH transfer function; **d)** distribution of the strike angle; **e)** distribution of the dip angle; **f)** distribution of the ellipticity.

Note that the ground motion is polarized (Fig. 1f) and almost horizontal around 4 Hz (Fig. 1e), but not directional (Fig. 1d). Frequency of 4 Hz corresponds to 1D fundamental frequency of the site (Fig. 1c). Results of polarization analysis (Figs. 1e-f) thus indicate potential site effect.

Appendix F

Horizontal amplification on topography at selected broad-band stations of INGV seismic network

HORIZONTAL AMPLIFICATION ON TOPOGRAPHY AT SELECTED BROAD-BAND STATIONS OF INGV SEISMIC NETWORK

Pischiutta et al. (2011) performed a systematic investigation on 226 rock site stations in Italy to estimate the site amplification of the horizontal motion and its tendency to be directional. Their analysis method combines H/V spectral ratios in the frequency domain (Nakamura, 1989) and assessment of the horizontal polarization angle in the time domain. Using the large data set of the Italian stations the first step of their analysis was the spectral characterization of one hour of calm ambient noise recorded at each station during the night, calculating the horizontal-to-vertical spectral ratios (HVSRs) for rotation angles of 10° to 180°. The mean spectral ratios plotted versus frequency and rotation angle are a powerful tool to display the occurrence, if any, of differential amplification of the horizontal motion along a specific azimuth (see Fig. 1). In Pischiutta et al. (2011), this tendency of many rock sites is also confirmed by the application of a time domain technique based on the covariance matrix method (Jurkevics, 1988). They repeated the analysis using seismic events, selected among those occurred in Italy in the period January 2008 – March 2011, with magnitude higher than 3. They found a general consistency between results obtained by using ambient noise and earthquakes. Pischiutta et al. (2011) concluded that 30% of rock stations shows an horizontal amplification larger than 2 and this amplification is strongly directional. Many of stations that show this behavior are installed on topographic irregularities: it is known from the literature that instrumental observations of topographic effects indicate larger motions transversally to the elongation of the relief (Spudich et al., 1996; Massa et al., 2010; Pischiutta et al., 2010; Marzorati et al., 2011).

Here we show results of nine selected stations installed on topographic irregularities (ALJA, CERT, CLTB, ESLN, FIAM, ILLI, INTR, LADO, SGTA) showing directional amplification.

In Figure 1 we show a local-scale description for three stations. Panel A is relative to station CERT (Cerreto Laziale) located on the top of an elongated ridge with an elevation of 300 m from the valley and about 1 km wide. The topography isolines are drawn in the top-left inset. Below this inset, ambient noise polarization (cyan rose diagram) and earthquake polarization (red rose diagram) at station CERT are compared, the contour map of H/V spectral ratios is shown as well. On the Cerreto Laziale hill, predominant polarization is oriented N80°, there is a strict consistency between ambient noise and earthquake polarization, and the predominant azimuth is transversal to the hill major axis. Panel B is relative to station CLTB (Caltabellotta) located on the top of an elongated ridge, which is 600 m high from the valley and 1 km wide. The analysis performed on ambient noise (cyan rose diagram) and earthquakes (blue rose diagram) consistently reveals a polarization oriented N160°.

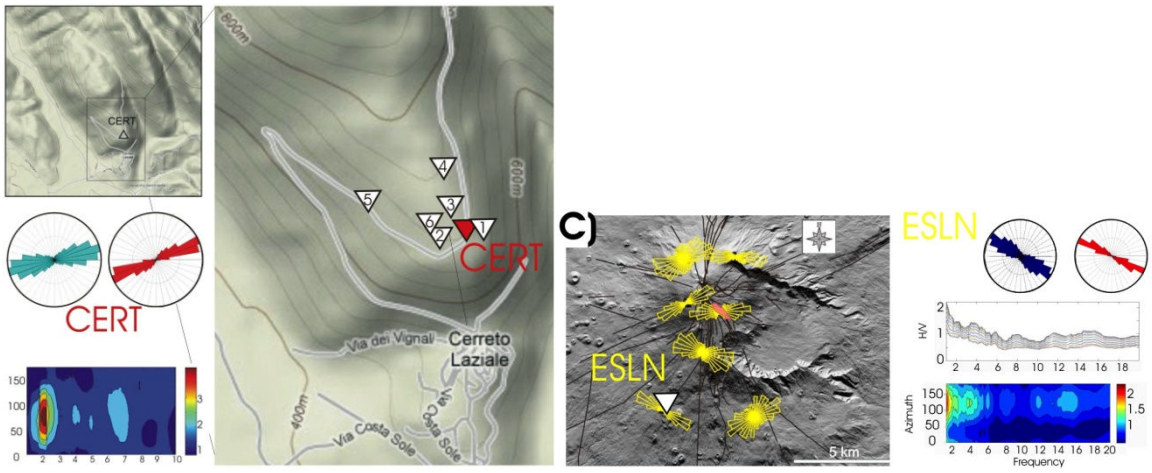

Fig. 1. Redrawn from Pischiutta et al. (2011). Results of polarization analysis for three representative stations and interpretation of results at the local-site scale. Panel A shows the polarization result at station CERT (Cerreto Laziale), on a 1 km wide and 300 m high ridge for ambient noise (cyan rose diagram) and seismic events (red rose diagram). In the middle, the array deployment is drawn on a DEM. In panel B, results of polarization at station CLTB (Caltabellotta) are illustrated. The H/V spectral ratios are shown on the left bottom, and the two rose diagrams represent polarization obtained from ambient noise (cyan rose diagram) and seismic events (blue rose diagram). Panel C describes observations at station ESLN, located on the top of Mt. Etna. The polarization pattern around the crater area was estimated by Falsaperla et al. (2010) that found a polarization orientation perpendicular to the radial fracture field. At ESLN, the result of our polarization analysis on ambient noise (blue rose diagram) and earthquake records (red rose diagram) confirms the site orientation previously found by Falsaperla et al. (2010).

Also in this case the polarization angle is perpendicular to the hill elongation. Finally, in panel C, an example of polarization on densely fractured rocks is shown. Results of polarization analysis (yellow rose diagrams) are from Falsaperla et al. (2010) who found that a fracture system produced by the 1989 volcanic activity on Mt. Etna strongly controls horizontal polarization at the crater stations. Among stations analyzed by Falsaperla et al. (2010), we consider ESLN which is part of the Italian Seismic Network (Fig. 1). Polarization derived from ambient noise (cyan rose diagram) and earthquake records (red rose diagram) are drawn with H/V spectral ratios. The horizontal polarization is oriented N120°, in agreement with Falsaperla et al. (2010): this direction is perpendicular to the local fracture system, that spreads radially from to the volcano crater. Station ESLN is an example of effects found in a volcanic context. Nevertheless in non-volcanic settings too the predominant fracture orientation has been recognized to affect polarization, with an orthogonal relation between fracture directions and observed polarization (Pischiutta et al., 2013).

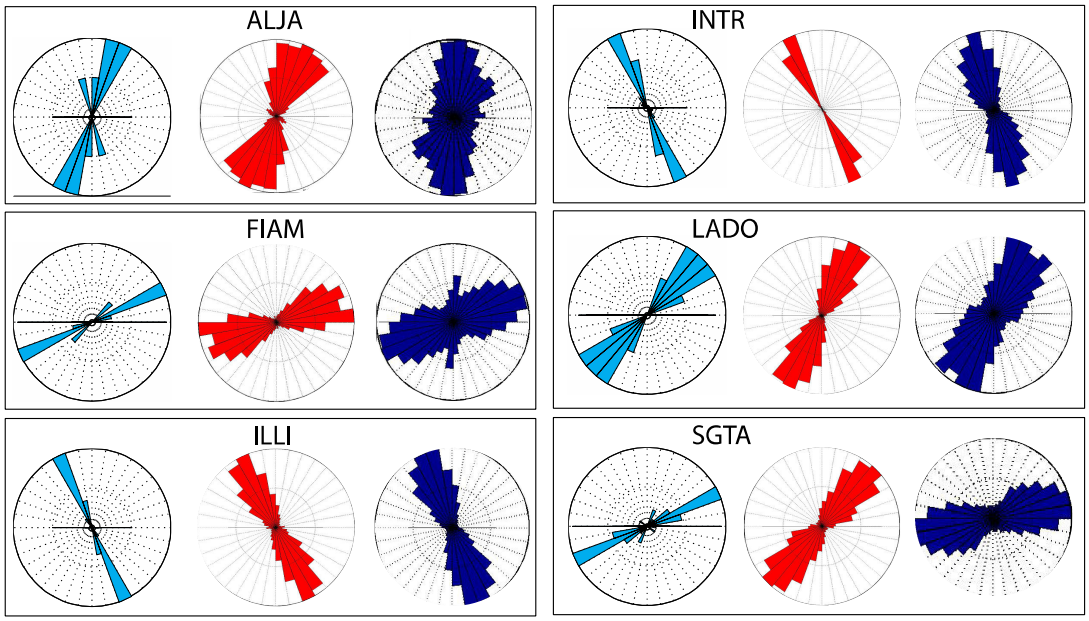

Fig. 2. Rose diagrams representing: rotation angles corresponding to the maximum-amplitude azimuths of response spectra (cyan); the horizontal polarization of ambient noise (red); the horizontal polarization of seismic events (blue).

During earthquakes, horizontal motion polarization can have a strong influence on the response of engineered structures, their rigidity too depending on azimuth. Measures of intensity shaking were proposed in the past to take into account the ground motion variability versus azimuth. Boore et al. (2006) defined GMRotDnn as response spectra obtained for period-dependent rotation angle, where nn is the fractile of the geometric means for rotation angles $0° < \theta < 180°$ sorted by amplitudes (e.g. GMRotD50 is the median value and GMRotD100 is the largest geometric mean over all rotation angles). Response spectra were computed for rotation angles from 10° to 180° with increments by 10°. In Fig. 2 we compare the maximum amplitude azimuth of response spectra (cyan rose diagram) with the horizontal polarization calculated by using ambient noise (red rose diagram) and seismic events (blue rose diagram at stations ALJA (Alia), FIAM (Fiamignano), ILLI (Lipari), INTR (Introdacqua), LADO (San Nicola dell'Alto) and SGTA (Sant'Agata di Puglia). We found that the maximum amplitude azimuth of response spectra calculated at each site on the recorded seismic events consistently agree with the mean horizontal polarization direction. The response spectra for the two orthogonal directions are compared with the GMPEs of not amplified rock sites assessed by Di Alessandro et al. (2008 and 2011). In Fig. 3 we show results at stations ALJA, FIAM, ILLI, INTR, LADO and SGTA as well as station locations on the Italian territory and epicenters of earthquakes used for the analysis. The red and black curves represent the maximum and minimum amplitude direction, respectively For the sake of comparison, the bleu curves represent the expected response spectrum and its + 1 s.d. uncertainty as derived by Di Alessandro et al. (2008 and 2011) using a site category (Class I) characterized by a flat (<2) H/V response spectra ratio.

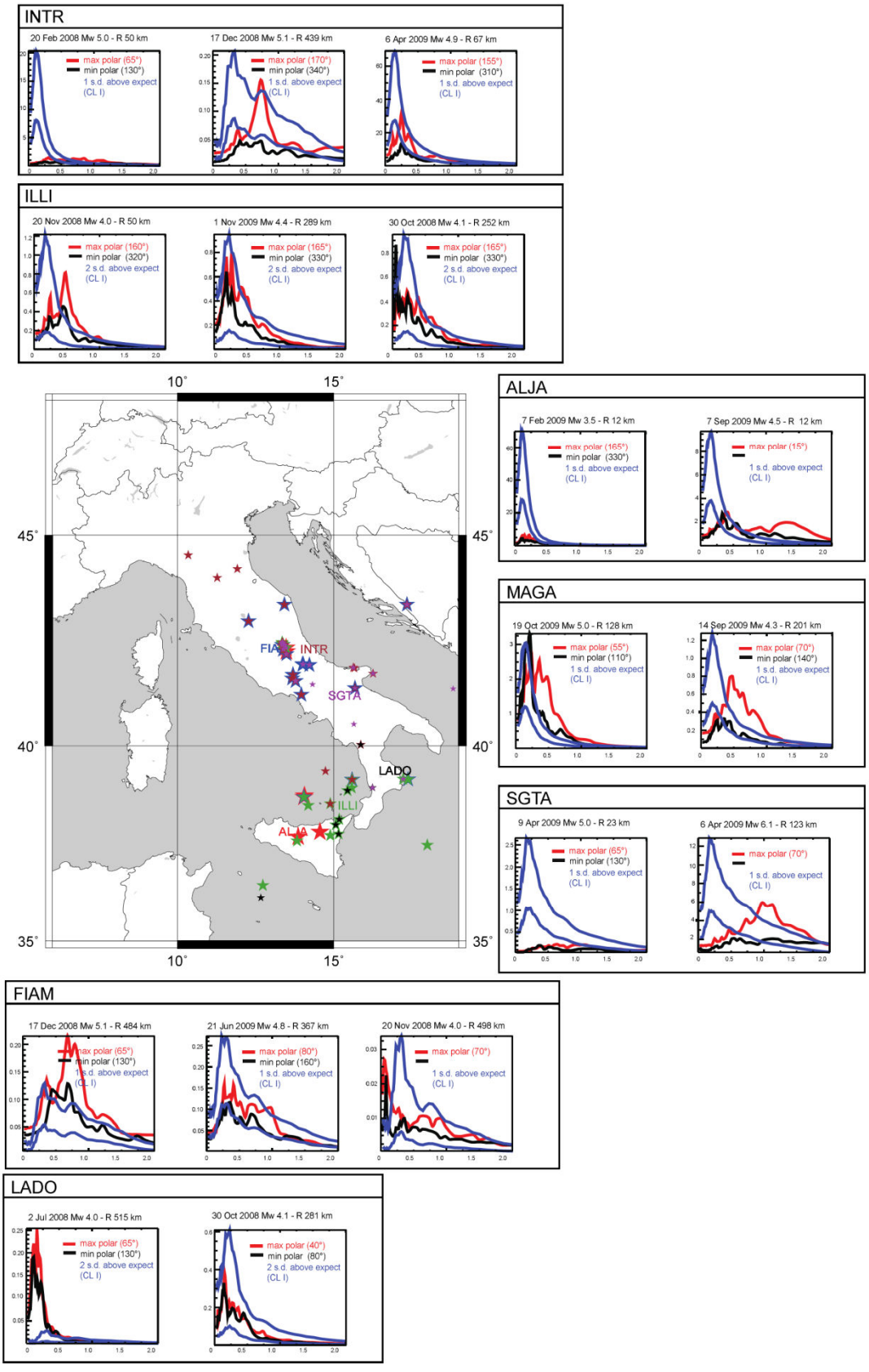

Fig. 3. Station locations on the Italian territory and epicenters of earthquakes used for the analysis Response spectra at rotation angles corresponding to the maximum- (red curve) and minimum-amplitude azimuths (black curves) of each station. The bleu colored band represents +1 s.d. above the expected curve of GMPEs by Di Alessandro et al. (2011) for class CL-I sites.

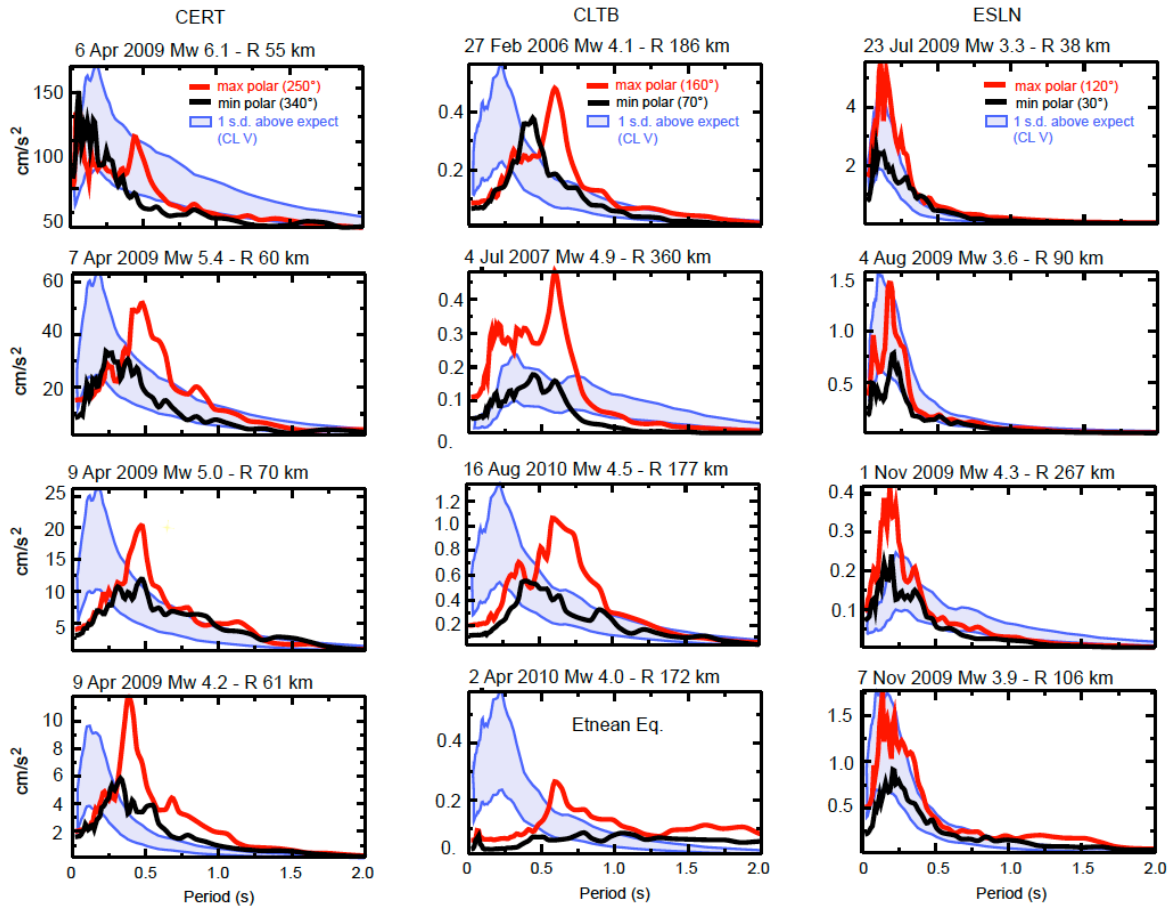

Fig. 4. Redrawn from Pischiutta et al. (2011). Response spectra at rotation angles corresponding to the maximum- (red curve) and minimum-amplitude azimuths (black curves) of each station. The bleu colored band represents +1 s.d. above the expected curve of GMPEs by Di Alessandro et al. (2011) for class CL-V sites. Note the anomaly of the long-period volcanic earthquake recorded at CLTB (bottom panel): it is poor in high-frequency content and rich in low frequencies, according to findings by Milana et al. (2009) for Etnean earthquakes.

Fig. 4 shows response spectra for the two orthogonal directions using available earthquake records (magnitude and distance of each earthquake are written in the figure) at stations CERT, CLTB and ESLN. Consistently to Fig. 3, response spectra in the minimum amplitude direction tend to lie within 1 s.d. above the expectation of GMPEs of not amplified rock sites. In contrast, ground motions of sites affected by directional effects tend to exceed the + 1 s.d. curve along the maximum amplitude direction. Often the excess is not limited to the fundamental site resonance but affects different period intervals: this is particularly evident at ESLN where both the 1-2 s site resonance and short ($T \approx 0.25$ s) periods are significantly amplified. The GMPEs assessed by Di Alessandro et al. (2008 and 2011) for sites classes depending on the site resonant period are also checked. This check is significant because the earthquake records of the test were not included in the data set used by Di Alessandro et al. (2011). Based on the H/V contour plots of Fig. 1, the class CL-III is assigned to CERT and CL-IV to CLTB and ESLN. Fig. 5 suggests that the ± 1 s. d. uncertainty (thin bleu lines) encompasses satisfactorily observations in terms of period-independent geometric mean and GMRotD50 as defined by Boore et al. (2006). Only response spectra along the maximum amplitude direction, in rare cases, exceed the + 1 s. d. curve.

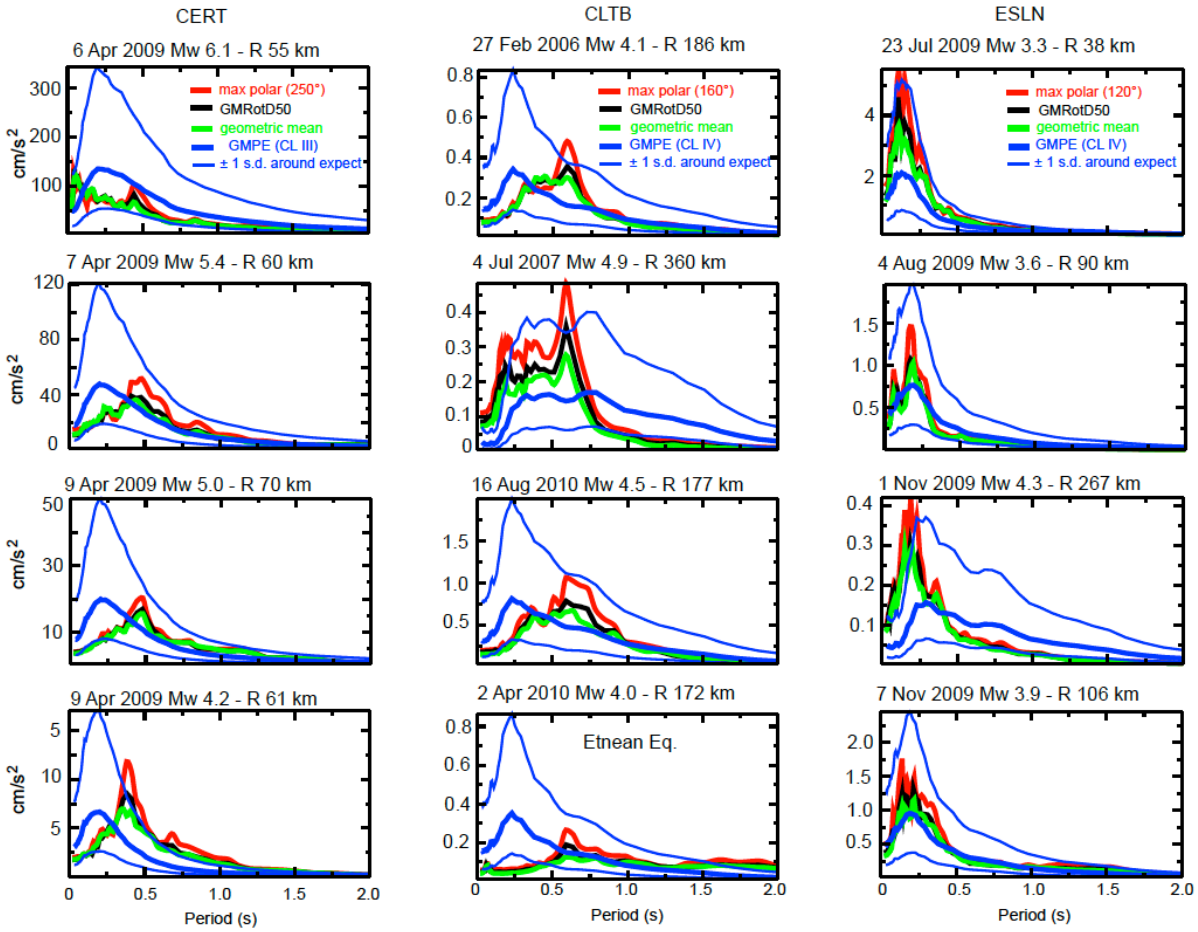

Fig. 5. Redrawn from Pischiutta et al. (2011). Response spectra of Fig. 2 are compared to expectations (thick bleu curves) of GMPEs by Di Alessandro et al. (2011) for class CL-III (CERT) and CL-IV (CLTB and ESLN). Thin bleu curves represent the ± 1 s. d. uncertainty around expectations.

REFERENCES

Boore, D.M., J. Watson-Lamprey, and N. A. Abrahamson [2006]. "Orientation-Independent Measures of Ground Motion," Bull. Seism. Soc. Am., Vol. 96, No. 4A, pp. 1502-1511.

Burjànek, J., G. Gassner-Stamm, V. Poggi, J.R. Moore, and D. Faeh [2010]. "Ambient vibration analysis of an unstable mountain slope", Geophys. J. Int., Vol. 180, pp. 820-828, doi: 10.1111/j.1365-246X.2009.04451.x.

Di Alessandro, C., L. F. Bonilla, A. Rovelli, and O. Scotti [2008]. "Influence of site classification on computing empirical ground-motion prediction equations in Italy", Proc. of the AGU Fall Meeting, San Francisco, CA, USA, 15-19 December 2008, paper n. S12A-05.

Di Alessandro, C., L. F. Bonilla, D. M. Boore, A. Rovelli, and O. Scotti [2011]. "Predominant-period Site Classification for Response Spectra Prediction Equations in Italy", Bull. Seismol. Soc. Am. (submitted).

Falsaperla, S., F. Cara, A. Rovelli, M. Neri, B. Behncke, and V. Acocella [2010]. "Effects of the 1989 fracture system in the dynamics of the upper SE flank of Etna revealed by volcanic tremor data: The missing link?", J. Geophys. Res., Vol. 115, B11306, doi:10.1029/ 2010JB007529.

Jurkevics, A. [1988]. "Polarization analysis of three component array data", Bull. Seism. Soc. Am., Vol. 78, pp. 1725-1743.

Marzorati S., C. Ladina, E. Falcucci, S. Gori, M. Saroli, G. Ameri, F. Galadini [2011]. “Site effects on the rock: the case of Castelvecchio Subequo (L’Aquila, central Italy)”, Bull. Earthquake Eng., Vol. 9, pp. 841–868, doi: 10.1007/s10518-011-9263-5.

Massa, M., S. Lovati, E. D’Alema, G. Ferretti, and M. Bakavoli [2010]. “An experimental approach for estimating seismic amplification effects at the top of a ridge, and the implication for ground-motion predictions: the case of Narni, central Italy”, Bull. Seism. Soc. Am., Vol. 100, No. 6, pp. 3020–3034, doi: 10.1785/0120090382.

Milana, G., A. Rovelli, A. De Sortis, G. Calderoni, G. Coco, M. Corrao, and P. Marsan [2008]. "The role of long-period ground motions on magnitude and damage of volcanic earthquakes on Mt. Etna, Italy”, Bull. Seism. Soc. Am., Vol. 98, No. 6, pp. 2724–2738, doi: 10.1785/0120080072.

Nakamura, Y. [1989]. A method for dynamic characteristics estimation of subsurface using microtremors on the ground surface, Quarterly Rept. RTRI, Japan., Vol. 30, pp. 25-33.

Pischiutta, M., G. Cultrera, A. Caserta, L. Luzi, and A. Rovelli [2010]. “Topographic effects on the hill of Nocera Umbra, central Italy”, Geophys, J. Int., Vol. 182, No. 2, pp. 977–987, doi: 10.1111/j.1365-246X.2010.04654.x.

Pischiutta, M., A. Rovelli, P. Vannoli and G. Calderoni [2011]. “Recurrence of horizontal amplification at rock sites: a test using H/V based ground motion prediction equations”, 4th IASPEI / IAEE International Symposium, Santa Barbara (CA), August 23-26.

Pischiutta, M., Rovelli, A., Salvini, F., Di Giulio, G. and Y. Ben-Zion [2013]. “Directional resonance variations across the Pernicana Fault, Mt Etna, in relation to brittle deformation fields”, Geophys, J. Int., doi:10.1093/gji/ggt031.

Spudich, P., M. Hellweg, and W. H. Lee [1996]. “Directional topographic site response at Tarzana observed in aftershocks of the 1994 Northridge, California, earthquake: Implication for main shock motion”, Bull. Seismol. Soc. Am., Vol. 86, pp. 193–208.